N81-77511

N83-30428

NASA Contractor Report 165748

AERODYNAMIC EVALUATION OF CIRCULATION CONTROL PROPELLERS

Albert L. Braslow

THE BIONETICS CORPORATION
18 Research Drive
Hampton, Virginia 23666

Contract NAS1-14970
June 1981

National Aeronautics and
Space Administration

Langley Research Center
Hampton, Virginia 23665

TABLE OF CONTENTS

SECTION	PAGE
SUMMARY	1
INTRODUCTION	2
SYMBOLS AND COEFFICIENTS	4
RESULTS AND DISCUSSION	8
CC Airfoil Selection	8
CC Airfoil Application to Propeller	11
Derivation of propeller aerodynamic relationships	12
Characteristics of selected general aviation airplane	14
CC propeller calculations and comparisons	15
Compressibility effects	20
CONCLUDING REMARKS	24
REFERENCES	27
APPENDIX A	28
APPENDIX B	31
ADDENDUM	34
APPENDIX C	37

LIST OF TABLES

TABLES		PAGE
I	Geometry of Basic Airplane and Winglets	39
II	3-Bladed CC-Elliptical Airfoil Propellers	41
III	3-Bladed CC-Supercritical Airfoil Propeller	42

LIST OF FIGURES

FIGURES		PAGE
1	Reference Planes for the Momentum Equation	43
2	Schematic of CC Airfoil Drag Coefficient Breakdown	44
3	Subsonic Model Geometries	45
4	Variation of Airfoil Total Drag Coefficient with Airfoil Lift Coefficient for Rounded 15-Percent Chord Thick Ellipse	46
5	Variation of Airfoil Total Drag Coefficient with Airfoil Lift Coefficient for Modified 15-Percent Chord Thick Ellipse	47
6	Variation of Airfoil Lift Coefficient with Angle of Attack for Rounded 15-Percent Chord Thick Ellipse	48
7	Variation of Airfoil Total Drag Coefficient with Airfoil Angle of Attack for Rounded 15-Percent Chord Thick Ellipse	49
8	Variation of Airfoil Lift/Drag Ratio with Angle of Attack for Rounded 15-Percent Chord Thick Ellipse	50
9	Propeller Blade Element Definitions	51
10	Thrust and Torque Grading Curves	52
11	General Layout of Test Airplane	53
12	Variation of Selected Airplane Lift Coefficient with Airplane Drag Coefficient	54
13	Variation of Basic Propeller Power Coefficient with Advance Ratio for Selected Airplane	55
14	Altitude Performance Curves for Selected Airplane Engine	56

LIST OF FIGURES

FIGURES		PAGE
15	Fuel Flow Characteristics for Selected Airplane Engine	57
16	Variation of Selected Airplane Lift and Drag Coefficients with Airplane Velocity	58
17	Variation of Selected Airplane Required Thrust with Airplane Velocity	59
18	Variation of Ratio of Jet Velocity at Ambient Pressure to Reference Velocity with Jet Momentum Coefficient for Rounded 15-Percent Chord Thick Ellipse	60
19	Variation of Selected Airplane Propeller Power Coefficient and Thrust Coefficient with Propeller Efficiency	61
20	Variation of Airfoil Total Drag Coefficient with Angle of Attack for 15-percent chord thick CC-Supercritical Airfoil	62
21	Variation of Airfoil Lift/Drag Ratio with Angle of Attack for 15-percent Chord Thick CC-Supercritical Airfoil	63
22	Variation of Ratio of Jet Velocity at Ambient Pressure to Reference Velocity with Jet Momentum Coefficient for 15-percent Chord Thick CC-Supercritical Airfoil	64
A.1	Reference Planes for the Momentum Equation	65
A.2	Schematic of CC Airfoil Drag Coefficient Breakdown . .	66

SUMMARY

A first-order evaluation of the aerodynamic performance of propellers utilizing circulation control (CC) in place of variable pitch has been made. The concept is to provide the necessary changes in propeller thrust through controlled tangential blowing near a blunt trailing edge (Coanda effect) rather than through changes in propeller blade angle. The aerodynamic compatibility of CC propellers with the performance characteristics and requirements of a 1,600 kg (3600 lb) single-engine variable-pitch propeller general aviation airplane was evaluated.

The initial results with elliptical-shaped CC airfoils indicated that the feasibility of application to fixed-pitch propellers was doubtful for the class of airplane investigated (cruise speed of about 300 km/hr) and improbable for higher-speed airplanes. Supplemental data for a cambered circulation-control supercritical airfoil, which became available after completion of the initial evaluation, were subsequently analyzed and are included in the Addendum to this report. With the much superior aerodynamic characteristics of the CC-supercritical airfoil, elimination of variable pitch appears aerodynamically feasible for low-speed airplanes through the use of a moderate amount of upper-surface blowing near the trailing edge during cruise. Overall feasibility depends upon results of structural and systems-type analyses.

INTRODUCTION

A jet of air blown tangentialy over the upper surface of an airfoil near a deliberately rounded trailing edge produces increased lift at a fixed geometric angle of attack. This phenomenon of increased lift, or circulation around the airfoil, results from the ability of the blown jet to remain attached to a convex curved surface through considerable deflection angles, the well-known Coanda effect. Circulation control (CC) airfoils, as these blunt-based blown airfoils are known, have been considered for various applications, e.g., V/STOL aircraft wings, helicopter rotors, submarine stern planes, and lifting fans for surface-effect ships.

A suggestion has been made that perhaps fuel consumption and/or total life cost advantages would accrue for some general aviation airplanes with the application of CC airfoils to propellers in place of variable propeller-pitch mechanisms. The required changes in propeller thrust through the airplane speed range could be obtained with a constant-pitch CC propeller by changes in blown-jet mass flow rate rather than by changes in propeller blade angle. A prudent approach towards determination of the overall feasibility of this concept appeared to be to determine first the aerodynamic compatibility of a CC propeller with airplane performance requirements before undertaking any detailed aerodynamic, structural, and systems design of a CC propeller.

The results of a first-order aerodynamic analysis are covered in this report. Included are selection of a candidate CC airfoil for propeller application based on review and analysis of data available in the CC-airfoil literature, derivation of simplified relationships required for application of CC airfoils to propellers,

estimates of CC-propeller aerodynamic characteristics as applied to a selected general aviation airplane, and aerodynamic comparison of CC propellers with that of the variable-pitch propeller installed on the selected airplane.

SYMBOLS AND COEFFICIENTS

a	speed of sound, m/s (ft/sec)
A	area, m^2 (ft^2)
B	number of propeller blades
b	blade element chord length, m (ft)
C_D	airplane drag coefficient, $\frac{D}{q_\infty S_W}$
C_L	airplane lift coefficient, $\frac{L}{q_\infty S_W}$
c	airfoil chord length, m (ft)
c_{d_T}	airfoil total drag coefficient, $\frac{d_T}{q_\infty S}$
c_ℓ	airfoil or blade element lift coefficient, $\frac{\ell}{q_\infty S}$
c_μ	momentum coefficient, $\frac{\dot{m}_j V_j}{q_\infty S}$
C_p	propeller power coefficient, $\frac{P}{\rho_\infty n^3 D^5}$ and specific heat at constant pressure, $m^2/sec^2\ {}^oK$ ($ft^2/sec^2\ {}^oR$)
C_T	propeller thrust coefficient, $\frac{T}{\rho_\infty n^2 D^4}$
d_T	airfoil total drag, N (lb) = $d_W + d_j + d_{pe}$
d_j	jet drag, N (lb)
d_{pe}	drag equivalent of blowing power, N (lb)
d_W	wake drag, N (lb)
D	propeller diameter, m (ft) and airplane drag, N (lb)

E	total energy, N-m (lb-ft)
f	blade element drag force, N (lb)
F	force, N (lb)
h	altitude, km (ft) and blowing slot height, mm (inches)
H	total pressure, N/m^2 (lb/ft^2)
HP	horsepower, 746 watts ($\frac{550 \text{ ft-lbs}}{\text{sec}}$)
J	propeller advance ratio, $\frac{V_\infty}{nD}$
ℓ	airfoil or blade element lift, N (lb)
L	airplane lift, N (lb)
m	mass, kg (slug)
$\dot{m}$	mass flow, kg/sec (slugs/sec)
M	Mach number
n	propeller rotational speed, rev/sec
P	static pressure, N/m^2 (lb/ft^2) and power, watts ($\frac{\text{ft-lbs}}{\text{sec}}$)
P_T	total pressure, N/m^2 (lb/ft^2)
q	dynamic pressure, N/m^2 (lb/ft^2)
Q	quantity flow, m^3/sec (ft^3/sec) and propeller torque, N-m (ft-lb)
Q_c	$\frac{c_\ell \, b \, r \sin(\phi + \gamma)}{\sin^2 \phi \cos \gamma}$, m^2 (ft^2)
r	propeller radius at a blade element, m (ft)
R	propeller radius at propeller tip, m (ft) and resultant force on propeller blade element, N (lb) and gas constant, $m^2/sec^2 \, {}^oK$ ($ft^2/sec^2 \, {}^oR$)
R_c	Reynolds number based on airfoil chord, $\frac{\rho_\infty V_\infty c}{\mu_\infty}$

S	airfoil reference area, c x 1, m^2 (ft^2)
S_w	airplane wing reference area, m^2 (ft^2)
T	static temperature, ^oK (^oR) and propeller thrust, N (lb)
T_c	$\frac{c_\ell \, b \cos(\phi + \gamma)}{\sin^2 \phi \cos \gamma}$ m (ft)
v, V	velocity, m/sec (ft/sec)
W	airplane gross weight, kg (lb)
x	relative free-stream direction and distance along airfoil chord from leading edge, m (ft)
α	airfoil or blade element angle of attack, deg
β	see Figure 7
γ	see Figure 7 and ratio of specific heats
η	propeller efficiency, $(\frac{C_T}{C_p})(\frac{V_\infty}{nD})$
μ	viscosity, N sec/m^2 (lb sec/ft^2)
ρ	density, kg/m^3 (slugs/ft^3)
ϕ	see Figure 7

Subscripts

ave	average
avail	available
comp	compressor
j	jet
max	maximum
n	local condition
r	relative to blade element
rake	as measured by downstream instrumentation
reqd	required
w	wake
x	relative free-stream direction
.75R	blade element at 75-percent tip radius
∞	free stream or ambient

RESULTS AND DISCUSSION

CC Airfoil Selection

The most complete series of experimental data on circulation control (CC) airfoils with potential for application to airplane propellers has been obtained by the David W. Taylor Naval Ship Research and Development Center (NSRDC). These data were obtained principally for airfoils with elliptical shapes and ellipses with modified trailing-edge shapes. Most of the data were obtained at low subsonic speeds with a limited amount of information at high subsonic speeds. Airfoil drag measurements were made with a rake of total head tubes behind the airfoil and included the momentum of the air ejected from the tangential slot.

The experimental data available on CC ellipses and modified ellipses include thicknesses of 10 -, 15 -, 20 -, and 30 -percent chord. The 15 - percent thick airfoil was considered for application to a propeller to maintain sufficient thickness for structural and air ducting purposes and to permit a sufficiently blunt trailing edge to yield good Coanda turning. At the same time, adverse compressibility effects that would occur at the high subsonic propeller tip speeds are limited. Furthermore, more data were available for various 15 - percent chord thick sections than for the other sections. The basic data used for the current feasibility study were obtained from reference 1 for a "pure" ellipse and a "rounded" ellipse and from unpublished data obtained from the author of reference 1 for a "modified" ellipse with a trailing-edge radius larger than for the "rounded" ellipse.

Drawings of the three configurations tested are presented in Figure 1. Data for a 0.25 mm (0.01 inch) high jet slot, the optimum configuration tested, were used. The slot was located at 96-percent chord for the rounded and modified ellipses and slightly forward (92.4-percent chord) for the pure ellipse due to a slightly longer chord (constant x position of slot). Reference 1 indicates that both maximum lift coefficient and lift to drag ratio through a large range of angle of attack are greater for the rounded ellipse than for the pure ellipse. The supplemental data provided by the NSRDC on the modified ellipse indicated even higher lift-drag ratios at large values of c_ℓ but lower lift-drag ratios than for the rounded ellipse at values of c_ℓ required for propeller sections.

The basic drag coefficients presented by the NSRDC represented the measured rake drag coefficients with a jet momentum flow "correction", i.e., $c_{d_{rake}} - c_\mu \left(\frac{V_\infty}{V_j} \right)$. In the application of a blown airfoil to an airplane propeller, the power required to blow the air must be accounted for and can be charged either to the power source (in this case the propulsion engine) or the airfoil itself. To provide a more realistic comparison of the aerodynamic characteristics of CC air foils as well as that of CC airfoils with unblown airfoils, the latter approach was selected, i.e., the "corrected" rake drag coefficients were converted to drag coefficients that include the drag equivalent of the blowing power required, as derived in Appendix A. The airfoil total drag coefficient, derived in Appendix A, is:

$$c_{d_T} = c_{d_{rake}} + \frac{c_\mu}{2} \left[\left(\frac{V_\infty}{V_j} \right) + \left(\frac{V_j}{V_\infty} \right) \right] .$$

Therefore, $c_{d_T} = \left[c_{d_{rake}} - c_\mu \left(\frac{V_\infty}{v_j} \right) \right] + 1.5\, c_\mu \left(\frac{V_\infty}{v_j} \right) + \frac{c_\mu}{2} \left(\frac{v_j}{V_\infty} \right)$.

A further comparison of the rounded and modified ellipses was made after conversion of the basic drag data to the total drag coefficient. These results are presented in Figures 2 and 3 for the rounded and modified ellipses, respectively.

For both of these CC airfoils, the data presented were obtained at a chord Reynolds number R_c of about 0.5×10^6 with smooth airfoil surfaces. The low Reynolds number and smooth surfaces permitted the possible attainment of some laminar flow, depending upon the turbulence level of the wind tunnel. The values of $(\ell/_d)_{max}$ obtained were from 38 to 41. With fully turbulent flow, the values of $(\ell/_d)_{max}$ would be lower, even at considerably larger Reynolds numbers. For comparison, the drag polar for an unblown NACA 65_2 - 015 airfoil (reference 2) at a chord Reynolds number of 6×10^6 with fully turbulent flow over both surfaces is plotted in Figure 3. This 15-percent chord thick unblown airfoil was selected rather than the NACA 0012 (12-percent chord thick) airfoil previously used in the literature for comparison in order to avoid the effects of a difference in thickness ratio. The value of $(\ell/_d)_{max}$ for the turbulent unblown airfoil is 50. For smooth surfaces at the same R_c of 6×10^6, reference 2 indicates a value of $(\ell/_d)_{max}$ greater than 90. It is apparent that care must be taken in comparisons of airfoils to account for differences in position of boundary-layer transition and in Reynolds number. Figure 3 also

indicates that at all lift coefficients lower than $c_{\ell\ max}$ of the unblown airfoil, the unblown airfoil has greater aerodynamic efficiency ($\ell/_d$) than the CC airfoils. This is expected because of the increased base drag of the blunter trailing-edge CC airfoil at low blowing coefficients and an increase in blowing-power drag with increased blowing. The advantage of circulation control is to increase $c_{\ell\ max}$ to values greater than attainable with unblown airfoils or to provide variations in lift coefficient at a constant angle of attack, as desired for a fixed-pitch propeller. The latter advantage, however, can only be obtained with a penalty in aerodynamic efficiency at the low to moderate values of lift coefficient required for propeller sections.

A comparison of the rounded and modified elliptical airfoils at the lower values of c_ℓ indicate a small aerodynamic efficiency advantage of the rounded ellipse as compared with the modified ellipse. This also is to be expected because the rounder-based "modified" shape produces higher drag at the low values of c_μ required. For other applications requiring larger lift, the "modified" shape would probably be superior. The "rounded" ellipse was selected, therefore, for further analysis in a propeller. The aerodynamic characteristics of the 15-percent chord thick rounded ellipse used in the propeller analysis are presented as a function of airfoil angle of attack, through the test range of mass-flow coefficient, in Figures 4, 5, and 6.

CC Airfoil Application to Propeller

The design of an efficient aircraft propeller is a complicated procedure involving many variables. Although an extensive data base and usually proprietary computer programs have been developed over the years for propeller

design, introduction of the additional blowing coefficient variable c_μ further complicates analysis of propellers with circulation control sections. A trial and error procedure with simplifying assumptions was used, therefore, to obtain a first-order indication of CC propeller performance. The assumptions used were optimistic to not unduly jeopardize the possible feasibility of CC propellers.

Derivation of propeller aerodynamic relationships. - For those unfamiliar with the aerodynamics of propellers, the following review of the aerodynamic relationships involved, according to the simple propeller blade element theory, should be beneficial. In the simple blade element theory, the aerodynamic forces on elementary strips of the propeller are considered and the forces on the elements are then added to obtain thrust and torque for the whole propeller. Each element of the propeller follows a helical path and can be treated as a section of a wing, i.e., two-dimensional wing section or airfoil. The simple blade-element theory ignores the induced inflow and swirl velocities in the plane of the propeller which must be considered in determination of the aerodynamic coefficients. However, in the comparison of the CC airfoils with conventional airfoils to produce like power absorption and thrust, disregarding the induced velocities will produce second-order errors. For the simple theory, Figure 7 presents the forces, velocities, and geometric relationships involved. The aircraft forward velocity is V_∞, the tangential velocity of the propeller element in the propeller plane is $2\pi rn$, where n is the propeller rotational speed (rps), and the resultant velocity of the element with respect to the air is V_r. The angle between the direction

of element motion and the plane of rotation is ϕ, the geometric angle between the blade element and the plane of rotation is β, the blade angle, and the aerodynamic angle of attack of the element relative to the air is $\alpha = \beta - \phi$.

$$\gamma = \tan^{-1}\left(\frac{d\,d}{d\,\ell}\right)$$

$$\phi = \tan^{-1}\left(\frac{V_\infty}{\pi\, nD}_{.75R}\right)$$

$$d\ell = \tfrac{1}{2}\,\rho_\infty\, V_r^2\; c_\ell\; b\; dr$$

$$dR = \frac{d\ell}{\cos\,\gamma}$$

$$dT = dR\,\cos\,(\phi + \gamma) = \frac{\tfrac{1}{2}\,\rho_\infty\, V_r^2\, c_\ell\, b\, dr\,\cos\,(\phi + \gamma)}{\cos\,\gamma}$$

$$V_r = \frac{V_\infty}{\sin\,\phi}$$

$$dT = \frac{\tfrac{1}{2}\,\rho_\infty\, V_\infty^{\,2}\, c_\ell\, b\, dr\,\cos\,(\phi + \gamma)}{\sin^2\,\phi\,\cos\,\gamma}$$

$$\text{Let } T_c = \frac{c_\ell\, b\,\cos\,(\phi + \gamma)}{\sin^2\,\phi\,\cos\,\gamma}$$

$$dT = q_\infty\, T_c\, dr$$

$$T = q_\infty\, B \int_0^R T_c\, dr \text{ where B = number of blades}$$

$$df = dR\,\sin\,(\phi + \gamma)$$

$$dQ = r\,df = r\,dR\,\sin\,(\phi + \gamma) = \frac{r\,\tfrac{1}{2}\,\rho_\infty\, V_r^{\,2}\, c_\ell\, b\, dr\,\sin\,(\phi + \gamma)}{\cos\,\gamma}$$

$$\text{Let } Q_c = \frac{c_\ell\, b\, r\,\sin\,(\phi + \gamma)}{\sin^2\,\phi\,\cos\,\gamma}$$

$$dQ = q_\infty\, Q_c\, dr$$

$$Q = q_\infty\, B \int_0^R Q_c\, dr$$

Horsepower absorbed by propeller or torque horsepower:

$$Q(HP) = \frac{2 \pi n Q}{550}$$

$$\eta = \frac{T V_\infty}{2 \pi n Q}$$

Although blade width, angle, and airfoil vary along a propeller, the blade element at 3/4 of the tip radius is usually representative of the total propeller. The variation of the coefficient T_c and the coefficient Q_c as a function of the propeller radius is usually very similar for most propellers. The variations of T_c and Q_c presented in Figure 8 were used, therefore, for the CC propeller analysis with the section characteristics of Figures 4 and 5 applied at 0.75R. As previously derived, $T = q_\infty B \int_0^R T_c \, dr$ and $Q = q_\infty B \int_0^R Q_c \, dr$ and integration of the curves of Figure 8 yields $T = q_\infty B T_{c_{ave}} R$ and $Q = q_\infty B Q_{c_{ave}} R$ where $T_{c_{ave}} = \frac{T_{c_{.75R}}}{1.835}$ and $Q_{c_{ave}} = \frac{Q_{c_{.75R}}}{1.853}$. In addition, a value of propeller chord length b at 0.75R equal to 0.062 D was used.

Characteristics of selected general aviation airplane. - A single-engine variable-pitch propeller general aviation airplane (reference 3) was selected for application of a fixed-pitch CC propeller. A three-view drawing of the airplane is presented as Figure 9 and the geometry is tabulated in Table I. Airplane drag polars (reference 4) for configurations with and without winglets, are presented in Figure 10 and the propeller power coefficient and efficiency characteristics in Figure 11. Engine characteristics are presented in Figures 12 and 13. Figure 14 presents the variation of airplane lift

coefficient C_L with velocity as calculated for a constant airplane gross weight of 1600 kg (3600 lb) for altitudes of 3.05 km (10,000 ft) and sea level and the corresponding variation of airplane drag coefficient C_D with velocity for the basic airplane without winglets (from Figure 10). Based on these drag characteristics, the thrust required for steady unaccelerated flight was calculated for the same altitudes (Figure 15). Two flight conditions were selected for CC propeller calculations and comparisons with the basic airplane propeller - 82.3 m/sec (270 ft/sec) cruise at 3.05 km (10,000 ft) altitude and 38.1 m/sec (125 ft/sec) steady-state flight at sea level.

CC propeller calculations and comparisons. - The approach taken was to assume the thrust and torque grading curves of Figure 8 for both the CC and basic airplane propellers. For the selected cruise flight condition, determine the required $T_{c_{.75R}}$ for the basic airplane from the thrust-required curve of Figure 15 and the previously derived equations. Through a trial and error procedure, determine a CC propeller configuration that provides the required thrust at cruise in terms of $T_{c_{.75R}}$ and then determine the equivalent horsepower required (including the incompressible blowing power). When a match is obtained at cruise, calculate the airplane performance at the low-speed low-altitude steady-state flight condition with the CC propeller blade pitch the same as determined for cruise. Additional calculations and comparisons, to be discussed later, were then made.

For the sake of brevity, only a sufficient number of the calculations made to indicate important trends and conclusions are presented. The initial CC propeller geometry analyzed had the same diameter, 2.13 m (7 ft) as the

basic propeller. Lines 2 and 3 of Table II indicate that with a propeller pitch angle β of 20° at the recommended cruise rpm of 2500, required thrust, as indicated by the value of $T_{c_{.75R}}$ for the basic airplane, is unattainable with the engine power available. Although an increase in β at cruise will decrease the power required through operation at a resultant α nearer maximum efficiency (Figure 6), the fixed-pitch requirement limits the allowable β to a value for which the low-speed α does not exceed some acceptable value. Lines 4 and 5 of Table II indicate that a β as large as the assumed value of 20° results in a value of α at 38.1 m/sec (125 ft/sec) of greater than 9° which is not only greater than the value for which CC-airfoil data are available but also is equal to or greater than the α for airfoil stall (Figure 4 and reference 2). The α at low speed was then arbitrarily limited to 6° and the corresponding β determined (line 6 of Table II). With this value of β, lines 7 and 8 of Table II indicate that required thrust at cruise can still not be attained within the power available. An attempt, therefore, was made to reduce the power required through reductions in propeller diameter. Calculations were made for diameters of 2.04, 1.98, 1.83 m (6.7, 6.5, and 6 ft). For the 1.83 m (6 ft) diameter case, results of which are also presented in Table II, the low-speed flight condition was investigated first; a maximum angle of attack of 6° was imposed again to avoid stall and to remain within the range of available data. As large an α as possible is desired at low speeds so that the resultant fixed β will yield an α at cruise speed a minimum amount lower than the α for maximum $\ell/_d$ (Figure 6). With the resultant value of β of 17.1° (line 9), cruise thrust was obtained at 2500 rpm (line 13) but still

at greater than available power. Because line 10 indicates that, with the imposed limiting value of α of 6^0, considerable thrust is available at low speed for climb and acceleration at less than available power, the blade angle β and, therefore, α was increased by 2^0. At cruise, the increased β resulted in a reduction in power required at cruise thrust (lines 15 and 16) to almost that available. Further refinements in propeller geometry and conditions would be expected to yield a match for the CC propeller but were not pursued further because the remaining discrepancy between the power required and power available is considered of small significance for the first-order approximation used.

More than enough thrust is available for steady-state low-speed flight without blowing at maximum rpm and within the engine power available (line 17, as obtained by extrapolation of CC-airfoil data to $\alpha = 8^0$). Use of blowing therefore, can provide additional thrust for climb and acceleration. The ratio of thrust available to thrust required for steady-state flight at maximum rpm and power at sea level was calculated to be about 2.9. (Compare the 1.83 m (6 ft) diameter CC-propeller $T_{c_{.75R}}$ of line 18 at about maximum power with the required $T_{c_{.75R}}$.) The thrust ratio available for the basic airplane was calculated to be 2.7, as follows:

D = 2.13m (7 ft), n = 2700 rpm, h = 0 km (ft), V_∞ = 38.1 m/sec (125 ft/sec)

P_{avail} = 285 HP, W = 1600 kg (3600 lb)

$$C_p = \frac{(HP)\ (550)}{\rho_\infty\ n^3\ D^5}$$

$$C_T = \frac{T}{\rho_\infty n^2 D^4}$$

$$\eta = \left(\frac{C_T}{C_p} \right) \left(\frac{V_\infty}{n D} \right)$$

$$J = \frac{V_\infty}{n D} = 0.40$$

$$C_p = \frac{(285)\ (550)}{(.002378)\ \left(\frac{2700}{60} \right)^3\ (7)^5} = 0.0430$$

From the propeller C_p vs J curves of Figure 11, $\eta = 0.745$

$$C_{T_{avail}} = \frac{\eta\ C_p\ n\ D}{V_\infty} = \frac{\eta\ C_p}{J} = 0.0801$$

For steady-state flight, $T_{req'd}$ = 1,540 N (347 lb).

$$\therefore C_{T_{req'd}} = \frac{347}{(.002378)\ \left(\frac{2700}{60} \right)^2\ (7)^4} = 0.0300$$

$$\frac{T_{avail}}{T_{req'd}} = \frac{C_{T_{avail}}}{C_{T_{req'd}}} = \frac{0.0801}{0.0300} = 2.7$$

Although the reduced-diameter CC propeller will provide comparable climb and acceleration performance as the basic propeller, the blowing required will produce an appreciable increase in noise at low altitudes due to a high jet exhaust velocity. An indication of the jet velocity can be obtained from a calculation of the propeller relative velocity $V_r = \frac{V_\infty}{\sin \phi}$ = 198 m/sec

(648 ft/sec) and the experimental data of Figure 16 that presents the fully-expanded jet velocity as a fraction of the relative velocity plotted against c_μ. For the c_μ at which full power is absorbed of about 0.008 (line 18), the value of $\frac{v_j}{V_r} \simeq 1.8$ with a resultant $v_j \simeq 355.4$ m/sec (1166 ft/sec).

Fuel consumption. - A comparison was made of the fuel consumption at cruise of the general aviation airplane with the basic propeller and with the 1.83 m (6 ft) diameter CC propeller. The fuel consumption for the basic propeller was obtained as follows:

$$J = \frac{V_\infty}{n\ D} = \frac{270}{\left(\frac{2500}{60}\right)(7)} = 0.93$$

From Figure 11 and the relationship $C_p = \frac{C_T\ J}{\eta}$, the variation of C_p and of C_T with η was obtained and plotted in Figure 17. For cruise at 82.3 m/sec (270 ft/sec) at 3.05 km (10,000 ft), $C_{T_{req'd}} = \frac{T}{\rho_\infty\ n^2\ D^4} =$

$$\frac{324}{(.001756)\left(\frac{2500}{60}\right)^2 (7)^4} = 0.0443.$$

At $C_{T_{req'd}} = 0.0443$, $\eta = 0.866$ from Figure 17 and $C_p = \frac{(.0443)\ (.93)}{.866} = 0.0476$

$\therefore$ Power $= \frac{C_p\ \rho_\infty\ n^3\ D^5}{550} = 185$ HP

From Figure 13, the fuel flow equals 35 kg/hr (77 lb/hr) $\simeq$ 0.0486 m^3/hr (12.83 gals/hr).

For the CC propeller at the same flight condition, the required power is the maximum available, 188 HP. From Figure 13, the fuel flow equals

36.1 kg/hr (79.5 lb/hr) $\simeq$ .0502 m^3/hr (13.25 gals/hr). The fuel consumption at cruise, therefore, is about 3.25% greater for the CC propeller than for the basic propeller. As a matter of interest, the efficiency of the CC propeller at the cruise condition is less than 0.83 as compared with the previously determined value of 0.866 for the basic propeller. The CC propeller efficiency was obtained from $\eta = \frac{T\ V_\infty}{2\ \pi\ n\ Q}$ where $T = q_\infty\ B\ T_{c_{ave}}$ and $Q = q_\infty\ B\ Q_{c_{ave}}\ R$ and, therefore, $\eta = \left(\frac{T_{c_{ave}}}{Q_{c_{ave}}}\right)\left(\frac{V_\infty}{2\ \pi\ n}\right)$.

Compressibility effects. - The airfoils towards the tips of airplane propellers operate at high subsonic relative velocities. Some high subsonic-speed data obtained on the 15 - percent chord thick "pure" ellipse and "rounded" ellipse are presented in reference 5. The results indicate that although the rounded ellipse selected for the current study had a lower maximum lift-drag ratio at high subsonic speeds than the pure ellipse, the aerodynamic efficiency of the pure ellipse was lower at high speeds than that of the rounded ellipse at low speeds. The deterioration of airfoil performance at high speeds was attributed to an increase in drag with blowing as a probable result of jet detachment. It is apparent from these results that, at least for those airfoils investigated, the low-speed data used in the current study are likely to be optimistic because of the adverse compressibility effects. Also, very limited information in reference 6 indicates that blowing through a choked jet exit, which will be the case for the propeller, was clearly less effective than blowing through a subsonic exit.

In addition to these compressibility effects on the external aerodynamic characteristics of the CC airfoils, it must be recalled that the drag equivalent of the blowing power required was calculated on the basis of incompressible flow assumptions. The blowing power required, when determined for compressible flow conditions, will be significantly higher than for incompressible flow. To provide an indication of the compressor characteristics required to pump the blown air, calculations were made with compressible flow relationships, derived in Appendix B, for cruise at 82.3 m/sec (270 ft/sec) at 3.05 km (10,000 ft) altitude with the recommended engine rpm of 2500. The basic parameters used are:

$R = 0.914$ m (3 ft), $b_{.75R} = 0.113$ m (.372 ft), $B = 3$

and $q_\infty = 3064$ N/m^2 (64 lb/ft^2), $\phi = 24.63^o$.

$\frac{V_j}{V_r} = 3.15$ at $c_\mu \simeq 0.22$ from line 16 of Table II and Figure 16.

Compressor capacity -

$V_r = \frac{82.3}{\sin \phi} = 198$ m/sec (648 ft/sec)

$v_j = 622.1$ m/sec (2041 ft/sec), $q_r = \frac{q_\infty}{\sin^2 \phi} = 17{,}641$ N/m^2 (368 lb/ft^2)

$c_\mu = \frac{\dot{m}_j \, v_j}{q_r \, b \times 1}$

$\dot{m}_j = \frac{(.022)(17{,}641)(.113)}{622.1} = .0705$ kg/sec (.0015 slug/sec) per unit span

$\dot{m}_j = 0.0705 \times$ span $\times$ 3 blades $= .19$ kg/sec (.0135 slug/sec) = (0.43 lb/sec)

Compressor compression ratio -

$$\frac{P_{T_j}}{P_{T_r}} = \left[\frac{1 - \left(\frac{P_\infty}{P_{T_r}} \right)^{\frac{\gamma-1}{\gamma}}}{\left(\frac{V_r}{V_j} \right)^2} + \left(\frac{P_\infty}{P_{T_r}} \right)^{\frac{\gamma-1}{\gamma}} \right]^{\frac{\gamma}{\gamma-1}}$$

at 3.05 km (10,000 ft), $T_r = 268^o$ K ($483\ ^oR$), $a = \sqrt{\gamma\ RT} = 328.3$ m/sec

(1077 ft/sec), $M_r = \frac{648}{1077} = 0.60$

$$\frac{P_\infty}{P_{T_r}} = \left(\frac{1}{1 + \frac{\gamma-1}{2} M_r^2} \right)^{\frac{\gamma}{\gamma-1}} = .784$$

$$\frac{P_{T_j}}{P_{T_r}} = \left[\frac{1 - (.784)^{.2857}}{\left(\frac{1}{3.15}\right)^2} + (.784)^{.2857} \right]^{3.5} = 5.17$$

Compressor power -

$$HP_{comp} = \frac{\dot{m}_j\ C_p\ T_{T_r}}{550} \left(\frac{T_{T_j}}{T_{T_r}} - 1 \right)$$

$$\frac{T_{T_j}}{T_{T_r}} = \left(\frac{P_{T_j}}{P_{T_r}} \right)^{\frac{\gamma-1}{\gamma}} = (5.17)^{.2857} = 1.60$$

$$C_p = 1004 \ \frac{N\text{-}m}{kg\ {}^{o}K} \ (6006 \ \frac{ft^2}{sec^2\ {}^{o}R}) \text{ for air}$$

$$T_{T_r} = T_r \left(1 + \frac{\gamma - 1}{2} M_r^2\right) = 268 \ (1 + .2 \times .6^2) = 287.3 \ {}^{o}K \ (517.8 \ {}^{o}R)$$

$$HP_{comp} = \frac{(.0135)\ (6006)\ (517.8)\ (1.60 - 1)}{550} = 45.8 \text{ for } \eta_{comp.} = 100\%$$

CONCLUDING REMARKS

A first-order hand-calculation method for analyzing a circulation control (CC) airfoil in a propeller was developed and used to define various CC propeller geometries for determination of their aerodynamic compatibility with the performance characteristics and requirements of a single-engine variable-pitch propeller general aviation airplane. Although the propeller geometries evaluated were not optimized configurations and were based on optimistic low-speed data and incompressible assumptions, it is believed that several reliable observations can be made.

A CC propeller of the same diameter as the basic airplane propeller selected, 2.13 m (7 ft), requires more power (including the power to pump the blown air) than that available at a cruise speed and altitude of 82.3 m/sec (270 ft/sec; 185 mph) and 3.05 km (10,000 ft). A CC propeller of about 1.83m (6 ft) diameter can provide the required cruise thrust at the engine power available. At low-speed flight 38.1 m/sec (85 mph) at low altitudes, a 1.83m (6 ft) diameter CC propeller provides a thrust margin for climb and acceleration of the same order as that provided by the basic propeller but with a supersonic blown-air jet velocity that will produce an appreciable increase in airplane noise.

Elimination of the variable-pitch mechanism, the reason for consideration of a CC propeller, requires CC-propeller operation at cruise at a propeller efficiency lower than that of the basic variable-pitch propeller. This result is principally due to the fact that the blade angle of attack at cruise speed

must be lower than the value for maximum lift/drag ratio in order to maintain to acceptable values the increased angle of attack that results at low speeds with a fixed blade pitch. The resultant fuel flow rate at cruise, therefore, was greater for the CC propeller than for the basic variable-pitch propeller. Differences in efficiencies and weights of the two operating systems will, of course, also affect the difference in fuel consumption.

The quantitative aerodynamic results calculated in this study were based on various optimistic assumptions. Low-speed aerodynamic data were used, whereas limited information indicates that the high subsonic speeds in the outboard regions of a propeller will cause significant adverse compressibility effects on the relatively thick 15 - percent chord CC airfoil analyzed. The data used were obtained with an unchoked jet exit, whereas blowing through a choked exit in the outboard propeller regions has been indicated to be less effective. The blown-air ducting system was assumed to be loss free and unconservative incompressible relationships were used in determination of the drag equivalent of the blowing power during the definition of possible propeller geometries. Determination of the compressor characteristics with more realistic compressible relationships indicate a rather large compressor is required even with an assumed 100 - percent efficiency. At cruise, an approximately 34 kw (46 horsepower) compressor was indicated as required to deliver about .19 kg/sec (0.4 lb/sec) of blown air through a pressure ratio of at least 7. It appears apparent, therefore, that the feasibility of application to fixed-pitch propellers of any of the circulation-control airfoils for which experimental data are currently

available is marginal at best for the class of airplanes investigated (cruise at about 300 km/hr) and improbable for higher-speed airplanes. Additional experimentation would be required to develop a combination of CC airfoil geometry, slot height, and slot location that provides the needed range of relatively low lift coefficient with reduced blowing power at the high subsonic-speed condition.

REFERENCES

1. Englar, Robert J.: Two-Dimensional Subsonic Wind Tunnel Tests of Two 15-Percent Thick Circulation Control Airfoils. NSRDC Technical Note AL - 211, August, 1971.

2. Abbott, Ira H. and von Doenhoff, Albert E.: Theory of Wing Sections Including a Summary of Airfoil Data. Dover Publications, Inc., New York, 1959.

3. Pilot's Operating Handbook and FAA Approved Airplane Flight Manual for the Beechcraft Bonanza A36 (E-927 and after). P/M 36-590002-17, Commercial Product Support, Beech Aircraft Corporation, October 1976 (Revised September 1979).

4. Holmes, B. J., von Dan, C. P., Brown, P. W., and Deal, P. L.: Flight Evaluation of the Effect of Winglets on Performance and Handling Qualities of a Single-Engine General Aviation Airplane. NASA TM 81892, December 1980.

5. Englar, Robert J.: Two-Dimensional Transonic Wind Tunnel Tests of Three 15-Percent Thick Circulation Control Airfoils. NSRDC Technical Note AL-182, December, 1970.

6. Englar, Robert J.: Experimental Investigation of the High Velocity Coanda Wall Jet Applied To Bluff Trailing Edge Circulation Control Airfoils. NSRDC Report 4708, September, 1975.

7. Harris, Charles D.: Aerodynamic Characteristics of a 14-Percent-Thick NASA Supercritical Airfoil Designed for a Normal-Force Coefficient of 0.7. NASA TM X-72712, July, 1975.

8. R. F. Englar, J. H. Nichols, Jr., M. J. Harris and G. Huson: Experimental Development of an Advanced Circulation Control Wing System for Navy STOL Aircraft. A1AA-81-0151 Aerospace Sciences Meeting, Jan. 1981, St. Louis, MO.

APPENDIX A

The momentum theorem can be applied to the airstream surrounding the airfoil as indicated by the control surface ABCD of Figure A. 1. The control surface is fixed to the airfoil with planes AD and BC located sufficiently far upstream and downstream so as to occur where the static pressure is equal to ambient. The planes AB and CD are far enough away from the airfoil so that the stream velocity in the x or drag direction is equal to V_∞. The momentum theory states that the rate of change of momentum through the control surface is equal to the sum of the applied external forces. Steady irrotational flow is assumed and for the purpose of determining drag, the external forces in the relative direction of motion (x) are considered:

$$\Sigma F_x = \oint V_x (\rho_n v_n) dA$$

With control surfaces AD + BC of equal area and the pressure everywhere equal to P_∞, the resultant force on the airfoil in the x direction is:

$$F_x = \int_{ABCD} V_x (\rho_n v_n) dA = \int_{AD} \rho_\infty V_\infty^2 dA - \int_{BC} \rho_n v_n^2 dA + \dot{m}_j V_\infty$$

From continuity,

$$\dot{m}_j + \int_{AD} \rho_\infty V_\infty dA = \int_{BC} \rho_n v_n dA$$

Then, $$F_x = \int_{AD} \rho_\infty V_\infty^2 dA - \int_{BC} \rho_n v_n^2 dA + V_\infty \int_{BC} \rho_n v_n dA - V_\infty \int_{AD} \rho_\infty V_\infty dA$$

$$= \int_{BC} \rho_n v_n (V_\infty - v_n) dA$$

Dividing the integral into wake and jet contributions,

$d = F_x = \int_{wake} \rho_w v_w (V_\infty - v_w) dA + \dot{m}_j (V_\infty - v_j)$ assuming uniform velocity across the jet.

Adding a drag equivalent of the power required, assuming no internal losses in the pumping system and 100% compressor efficiency,

$$d_T = d_w + d_j + d_{pe}$$

$$d_{pe} = \frac{Q\,(\Delta H)}{V_\infty} \quad \text{incompressible flow assumed}$$

$$= \left(\frac{\dot{m}_j}{\rho_\infty}\right)\left(\frac{\Delta H}{V_\infty}\right) = \frac{\dot{m}_j V_\infty \Delta H}{2\, q_\infty} = \frac{\dot{m}_j v_j}{2\, q_\infty}\left(\frac{V_\infty}{v_j}\right)(\Delta H)$$

$$= \frac{c_\mu S}{2}\left(\frac{V_\infty}{v_j}\right)(\Delta H), \text{ since } c_\mu = \frac{\dot{m}_j v_j}{q_\infty S}$$

$H_j = P_\infty + q_j$ and $H_\infty = P_\infty + q_\infty$

$$\Delta H = H_j - H_\infty = \tfrac{1}{2}\rho_\infty v_j^2 - \tfrac{1}{2}\rho_\infty V_\infty^2$$

$$d_{pe} = \frac{c_\mu S}{2}\left(\frac{V_\infty}{v_j}\right)\left(\frac{1}{2}\rho_\infty v_j^2 - \frac{1}{2}\rho_\infty V_\infty^2\right)$$

$$= \frac{c_\mu S}{2}\left(\frac{V_\infty}{v_j}\right)(q_\infty)\left[\left(\frac{v_j}{V_\infty}\right)^2 - 1\right] = \frac{c_\mu S\, q_\infty}{2}\left[\left(\frac{v_j}{V_\infty}\right) - \left(\frac{V_\infty}{v_j}\right)\right]$$

$$c_{d_{pe}} = \frac{d_{pe}}{q_\infty S} = \frac{c_\mu}{2}\left[\left(\frac{v_j}{V_\infty}\right) - \left(\frac{V_\infty}{v_j}\right)\right]$$

$$c_{d_T} = \frac{d_T}{q_\infty S} = c_{d_w} + \frac{\dot{m}_j V_\infty}{q_\infty S} - \frac{\dot{m}_j v_j}{q_\infty S} + \frac{c_\mu}{2}\left[\left(\frac{v_j}{V_\infty}\right) - \left(\frac{V_\infty}{v_j}\right)\right]$$

$$c_{d_{rake}} = c_{d_w} - \frac{\dot{m}_j v_j}{q_\infty S}$$

$$= c_{d_w} - c_\mu$$

$$c_{d_T} = c_{d_{rake}} + c_\mu\left(\frac{V_\infty}{v_j}\right) + \frac{c_\mu}{2}\left[\left(\frac{v_j}{V_\infty}\right) - \left(\frac{V_\infty}{v_j}\right)\right]$$

$$= c_{d_{rake}} + \frac{c_\mu}{2} \left(\frac{V_\infty}{v_j} \right) + \frac{c_\mu}{2} \left(\frac{v_j}{V_\infty} \right)$$

$$= c_{d_{rake}} + \frac{c_\mu}{2} \left[\left(\frac{V_\infty}{v_j} \right) + \left(\frac{v_j}{V_\infty} \right) \right]$$

A schematic representation of the various parts of a CC airfoil drag coefficient is presented in Figure A. 2.

APPENDIX B

For compressible adiabatic flow, the total energy equation is:

$$\frac{\text{Total energy, } E}{\text{mass, } m} = C_p T + \frac{V^2}{2} = C_p T_T$$

$$\text{Power} = \frac{\Delta E}{\Delta t} = \frac{m C_p \Delta T_T}{\Delta t} = \dot{m} C_p \Delta T_T \text{ where } \dot{m} = \frac{m}{\Delta t}$$

$$HP = \frac{\dot{m} C_p \Delta T_T}{550} \text{ since 1 HP = 550 ft-lb/sec}$$

$$HP_{\text{compressor}} = \frac{\dot{m}_j C_p}{550}\left(T_{T_j} - T_{T_r}\right) = \frac{\dot{m}_j C_p T_{T_r}}{550}\left(\frac{T_{T_j}}{T_{T_r}} - 1\right)$$

Find $\left(\frac{T_{T_j}}{T_{T_r}}\right)$:

Since $\frac{T_r}{T_{T_r}} = \left(\frac{P_r}{P_{T_r}}\right)^{\frac{\gamma-1}{\gamma}}$ and $\frac{T_j}{T_{T_j}} = \left(\frac{P_j}{P_{T_j}}\right)^{\frac{\gamma-1}{\gamma}}$ for adiabatic isentropic process

and $T_j = T_r$:

$$\frac{T_{T_j}}{T_{T_r}} = \left[\left(\frac{P_{T_j}}{P_j}\right)\left(\frac{P_r}{P_{T_r}}\right)\right]^{\frac{\gamma-1}{\gamma}}$$

and since $P_r = P_\infty = P_j$ for no losses and an unchoked jet exit:

$$\frac{T_{T_j}}{T_{T_r}} = \left(\frac{P_{T_j}}{P_{T_r}}\right)^{\frac{\gamma-1}{\gamma}}$$

Find $\left(\frac{P_{T_j}}{P_{T_r}}\right)^{\frac{\gamma-1}{\gamma}}$:

$$C_p \; T_{T_r} = C_p \; T_r + \frac{V_r^2}{2}$$

$$C_p \; T_{T_j} = C_p \; T_j + \frac{v_j^2}{2}$$

$$V_r = \left[2 \; C_p \; T_{T_r} \left(1 - \frac{T_r}{T_{T_r}} \right) \right]^{1/2}$$

$$v_j = \left[2 \; C_p \; T_{T_j} \left(1 - \frac{T_j}{T_{T_j}} \right) \right]^{1/2}$$

$$\frac{V_r}{v_j} = \left[\frac{T_{T_r} \left(1 - \frac{T_r}{T_{T_r}} \right)}{T_{T_j} \left(1 - \frac{T_j}{T_{T_j}} \right)} \right]^{1/2}$$

$$\left(\frac{V_r}{v_j}\right)^2 = \left(\frac{P_{T_r}}{P_{T_j}}\right)^{\frac{\gamma-1}{\gamma}} \left[\frac{1 - \left(\frac{P_r}{P_{T_r}}\right)^{\frac{\gamma-1}{\gamma}}}{1 - \left(\frac{P_j}{P_{T_j}}\right)^{\frac{\gamma-1}{\gamma}}} \right]$$

Since $P_r = P_\infty = P_j$

$$\left(\frac{V_r}{v_j}\right)^2 = \left(\frac{P_{T_r}}{P_{T_j}}\right)^{\frac{\gamma-1}{\gamma}} \left[\frac{1 - \left(\frac{P_\infty}{P_{T_r}}\right)^{\frac{\gamma-1}{\gamma}}}{1 - \left(\frac{P_\infty}{P_{T_j}}\right)^{\frac{\gamma-1}{\gamma}}}\right]$$

$$\left(\frac{V_r}{v_j}\right)^2 = \frac{1 - \left(\frac{P_\infty}{P_{T_r}}\right)^{\frac{\gamma-1}{\gamma}}}{\left(\frac{P_{T_j}}{P_{T_r}}\right)^{\frac{\gamma-1}{\gamma}} - \left(\frac{P_\infty}{P_{T_r}}\right)^{\frac{\gamma-1}{\gamma}}}$$

$$\left(\frac{P_{T_j}}{P_{T_r}}\right)^{\frac{\gamma-1}{\gamma}} = \frac{1 - \left(\frac{P_\infty}{P_{T_r}}\right)^{\frac{\gamma-1}{\gamma}}}{\left(\frac{V_r}{v_j}\right)^2} + \left(\frac{P_\infty}{P_{T_r}}\right)^{\frac{\gamma-1}{\gamma}}$$

and $\frac{P_\infty}{P_{T_r}} = \left(\frac{1}{1 + \frac{\gamma-1}{2} M_r^2}\right)^{\frac{\gamma}{\gamma-1}}$ isentropic perfect

ADDENDUM

After completion of this report, supplemental low-speed wind-tunnel results, recently obtained on a cambered circulation-control supercritical airfoil, was provided by the DTNSRDC. The airfoil tested was 17-percent chord thick with a blowing slot near a thickened trailing edge as shown in Figure 18, reference 8. The measured drag was reduced by DTNSRDC to provide characteristics equivalent to a 15-percent chord thick airfoil for comparison with the 15% thick elliptical airfoil previously analyzed. A small Reynolds number difference between the provided data and the propeller will have an insignificant effect on the propeller power calculations. Lift, drag, lift-drag ratio, and jet velocity characteristics are presented in Figures 19 to 22. The total drag coefficients are as defined in the previous analysis.

The CC-supercritical airfoil data were applied to the 3-bladed, 6-foot diameter propeller with the final results presented in Table III. The superior aerodynamic efficiency of this airfoil with and without blowing, compared with the elliptical CC airfoil, provided an entirely different result. As indicated in Table III, climb and acceleration performance exceeding that of the basic propeller can be obtained without blowing at maximum available power at the low-speed flight condition analyzed. With a constant blade pitch angle and a moderate amount of blowing, cruise thrust at the selected cruise condition can be obtained at engine power less than that required with the basic propeller (185 HP, from page 19). The latter

translates to a greater than 7% reduction in fuel usage during cruise, excluding that due to inefficiencies of the pumping system. A reasonable compressor of approximately 2.0 kw (2.6 horsepower), at 100% efficiency, delivering about 0.1 kg/sec (0.23 lb/sec) of blown air through a pressure ratio of about 1.24 is required. (See Appendix C). Because no blowing is required for climb and acceleration at the flight condition selected, no adverse noise is generated at this low-altitude condition as was the case for the elliptical CC airfoil.

Although some adverse effect of compressibility may be expected near the tip of the propeller, the magnitude of this effect with the CC-supercritical sections would appear to be minimal from the data of reference 7 for an unblown 14-percent chord thick cambered supercritical airfoil very similar to the CC-supercritical airfoil analyzed. The drag-rise Mach number at the lift coefficient used at cruise on the propeller at 75% radius exceeds 0.78 (Figure 8b of reference 7). The propeller relative Mach number at 75% radius at the selected cruise condition is 0.6. The propeller relative Mach number at the tip in cruise is 0.8. Possible adverse effects of blowing at the high relative subsonic speeds near the propeller tip should be investigated. These effects, however, are not expected to be prohibitive because the blown jet velocity at freestream static pressure is subsonic at 75% propeller radius and only slightly supersonic at the 6 ft-diameter propeller tip. (See Appendix C)

From the simplified analytical approach used, fixed-pitch high-performance supercritical-type CC-airfoil propellers appear aerodynamically compatible with

the performance requirements of low-speed general-aviation type airplanes. Establishment of the overall feasibility of fixed-pitch CC propellers for low-speed airplanes, however, requires structural and systems-type analyses. It is also possible that improved performance of the variable-pitch propeller can be obtained with higher performance unblown propeller sections.

APPENDIX C

15-PERCENT CHORD THICK CC-SUPERCRITICAL AIRFOIL ON 1.83 m (6 FT.) DIAMETER 3-BLADED PROPELLER

FUEL CONSUMPTION

From page 19, Basic prop: 12.83 gals/hr at 185 HP at h = 10,000 ft. and V_∞ = 270 ft/sec

CC prop: HP req at cruise 168.7

From Figure 13: Fuel required $\simeq$ 71 lb/hr $\simeq$ 11.83 gals/hr $\equiv$ about 7.8% reduction

COMPRESSOR CAPACITY

at c_μ = .0053, $\frac{V_j}{V_r} \simeq$ 1.4 (Figure 22)

$$V_r = \frac{V_\infty}{\sin \phi} = 197.5 \text{ m/sec (648 ft/sec)}$$

$$v_j = 276.5 \text{ m/sec (907 ft/sec)}$$

$$q_r = \frac{q_\infty}{\sin^2 \phi} = 17643 \text{ N/m}^2 \text{ (368.5 lb/ft}^2\text{)}$$

$$c_\mu = \frac{\dot{m}_j \, v_j}{q_r \, b \times 1}$$

$$\dot{m}_j = \frac{(.0053)\ (17643)\ (.113)}{276.5} = .0382 \text{ kg/sec per unit span of 1 m}$$
$$= .0008 \text{ slug/sec per unit span of 1 ft}$$

$$\dot{m}_j = .0382 \times \text{span} \times 3 \text{ blades} = .105 \text{ kg/sec (.0072 slug/sec)}$$
$$= .231 \text{ lb/sec}$$

COMPRESSOR COMPRESSION RATIO

From page 22,

$$M_r = 0.6$$

$$\frac{P_\infty}{P_{T_r}} = \left(\frac{1}{1 + \frac{\gamma-1}{2} M_r^2} \right)^{\frac{\gamma}{\gamma-1}} = .784$$

$$\frac{P_{T_j}}{P_{T_r}} = \left[\frac{1 - (.784)^{.2857}}{\left(\frac{1}{1.4}\right)^2} + (.784)^{.2587} \right]^{3.5} = 1.244$$

COMPRESSOR POWER

From page 22,

$$\text{HP comp} = \frac{\dot{m}_j C_p T_{T_r}}{550} \left(\frac{T_{T_j}}{T_{T_r}} - 1 \right)$$

$$\frac{T_{T_j}}{T_{T_r}} = \left(\frac{P_{T_j}}{P_{T_r}} \right)^{\frac{\gamma-1}{\gamma}} = (1.244)^{.2857} = 1.065$$

From page 23,

$$T_{T_r} = T_r \left(1 + \frac{\gamma - 1}{2} M_r^2\right) = 287.3^\circ \text{ K } (517.8^\circ \text{ R})$$

$$\text{HP comp} = \frac{(.0072)\ (6006)\ (517.8)\ (1.065 - 1)}{550} = 2.6 \text{ HP for } \eta = 100\%$$

Gross weight, N (lb)	16,013 (3,600)
Wing	
Area, m^2 (ft^2)	16.8 (181.0)
Wing loading, N/m^2 (lb/ft^2)	952 (19.9)
Span without winglets, m (ft)	10.21 (33.50)
Span with winglets (geometric), m (ft)	11.74 (35.05)
Aspect ratio without winglets (geometric)	6.20
Taper ratio	0.50
Airfoil section: root	NACA 23016.5 (modified)
tip	NACA 23012 (modified)
Root chord, m (in.)	2.13 (84.0)
Tip chord, m (in.)	1.07 (42.0)
Twist (washout), deg	3.0
Dihedral, deg	6.0
Incidence at root, deg	4.0
Sweep at half chord, deg	0
Winglet	
Length, m (in.)	0.91 (36.0)
Root chord, m (in.)	0.71 (28.0)
Tip chord, m (in.)	0.36 (14.0)
Area, m^2 (ft^2)	0.49 (5.25)
Aspect ratio	1.71

TABLE I: GEOMETRY OF BASIC AIRPLANE AND WINGLETS

Taper ratio	0.5
Sweep at quarter chord, deg	30.0
Twist, deg	0
Incidence at root, deg	-2.0
Cant angle, deg	15.0
Airfoil section	LS(1)-0413
Thickness ratio, perc of chord	13.0
Powerplant	
Manufacturer	Teledyne Continental Motors, Corp.
Model	IO-520-BA
Take-off and maximum continuous power, kW (hp)	213 (285)
Rpm	2700
Propeller	
Manufacturer	McCauley
Number of Blades	3
Hub type	3A32C76
Blade type	82NB-2

TABLE I: GEOMETRY OF BASIC AIRPLANE AND WINGLETS (concl'd)

	AIRPLANE CONDITIONS				PROP REQUIREMENTS		CC PROPELLER														BASIC ENGINE
Line	h km (1000 ft)	V_∞ m/sec (ft/sec)	q_∞ N/m^2 (lb/ft^2)	T N (lb)	$T_{c_{ave}}$	$T_{c_{.75R}}$	D m (ft)	β^o	n rpm	$\frac{V_\infty}{nD_{.75R}}$	ϕ^o	α^o	c_μ	c_ℓ	c_{d_T}	γ^o	$T_{c_{.75R}}$	$Q_{c_{.75R}}$	$Q_{c_{ave}}$	Q HP	HP avail
1	3.05 (10)	82.3 (270)	3064.3 (64)	1441 (324)	.482	.885	2.13 (7)	20	2500	1.234	21.45	-1.45	.007	.237	.0294	7.07	.681				
2	"	"	"	"	"	"	"	"	"	"	"	"	.008	.308	.0303	5.62	.894	1.200	.648	207	188
3	"	"	"	"	"	"	"	"	"	"	"	"	.0075	.273	.0299	6.25	.789	1.088	.587	188	"
4	0	38.1 (125)	891 (18.6)	1544 (347)			"	"	"	.571	10.31	9.69									
5	"	"	"	"			"	"	2700	.529	9.56	10.44									
6	"	"	"	"	1.777	3.260	"	15.56	"	"	"	6	0	.72	.024	1.91	7.019	3.655	1.972	170	285
7	3.05 (10)	82.3 (270)	3064.3 (64)	1441 (324)	.482	.885	"	"	2500	1.234	21.45	-5.89	.018	.328	.0396	6.88	.951	1.336	.721	231	188
8	"	"	"	"	"	"	"	"	"	"	"	"	.017	.287	.0384	7.62	.821	1.199	.647	207	"
9	0	38.1 (125)	891 (18.6)	1544 (347)	2.073	3.804	1.83 (6)	17.12	2700	.617	11.12	6	0	.72	.024	1.91	7.019	3.655	1.972	170	285
10	"	"	"	"	"	"	"	"	"	"	"	"	.01	1.2	.038	1.81	11.703	6.045	3.262	281	"
11	3.05 (10)	82.3 (270)	3064.3 (64)	1441 (324)	.563	1.03	"	"	2500	1.440	24.63	-7.51	.025	.422	.0495	6.69	.777				
12	"	"	"	"	"	"	"	"	"	"	"	"	.029	.597	.0555	5.31	1.113				
13	"	"	"	"	"	"	"	"	"	"	"	"	.028	.553	.054	5.58	1.03	1.347	.727	199	188
14	"	"	"	"	"	"	"	19.12	"	"	"	-5.51	.025	.663	.0497	4.29	1.25				
15	"	"	"	"	"	"	"	"	"	"	"	"	.0225	.56	.0459	4.69	1.05	1.326	.716	196	188
16	"	"	"	"	"	"	"	"	"	"	"	"	.022	.538	.0451	4.79	1.007	1.278	.690	189	"
17	0	38.1 (125)	891 (18.6)	1544 (347)	2.073	3.804	"	"	2700	.617	11.12	8	0	.7	.032	2.62	6.81	3.745	2.021	174	285
18	"	"	"	"	"	"	"	"	"	"	"	"	.008	1.148	.0544	2.71	11.16	6.182	3.336	287	"

TABLE II: 3-BLADED CC-ELLIPTICAL AIRFOIL PROPELLERS

AIRPLANE CONDITIONS				PROP REQUIREMENTS		CC PROPELLER															
h km (1000 ft)	V_∞ m/sec (ft/sec)	q_∞ N/m^2 (lb/ft^2)	T N (lb)	$T_{c_{ave}}$	$T_{c_{.75R}}$	D m (ft)	β°	n rpm	$\frac{V_\infty}{nD}_{.75R}$	ϕ°	α°	c_μ	c_{ℓ}	c_{d_T}	γ°	$T_{c_{.75R}}$	$Q_{c_{.75R}}$	$Q_{c_{ave}}$	Q HP	HP avail
0	38.1 (125)	891 (18.6)	1544 (347)	2.073	3.804	1.83 (6)	22.52	2700	.617	11.12	11.40	0	1.29	.0245	1.09	12.66	6.139	3.313	285	285
3.05 (10)	82.3 (270)	3064.3 (64)	1441 (324)	.563	1.03	1.83 (6)	22.52	2500	1.440	24.63	- 2.11	.0053	.535	.0150	1.606	1.03	1.140	.615	168.7	188

TABLE III: 3-BLADED CC-SUPERCRITICAL AIRFOIL PROPELLER

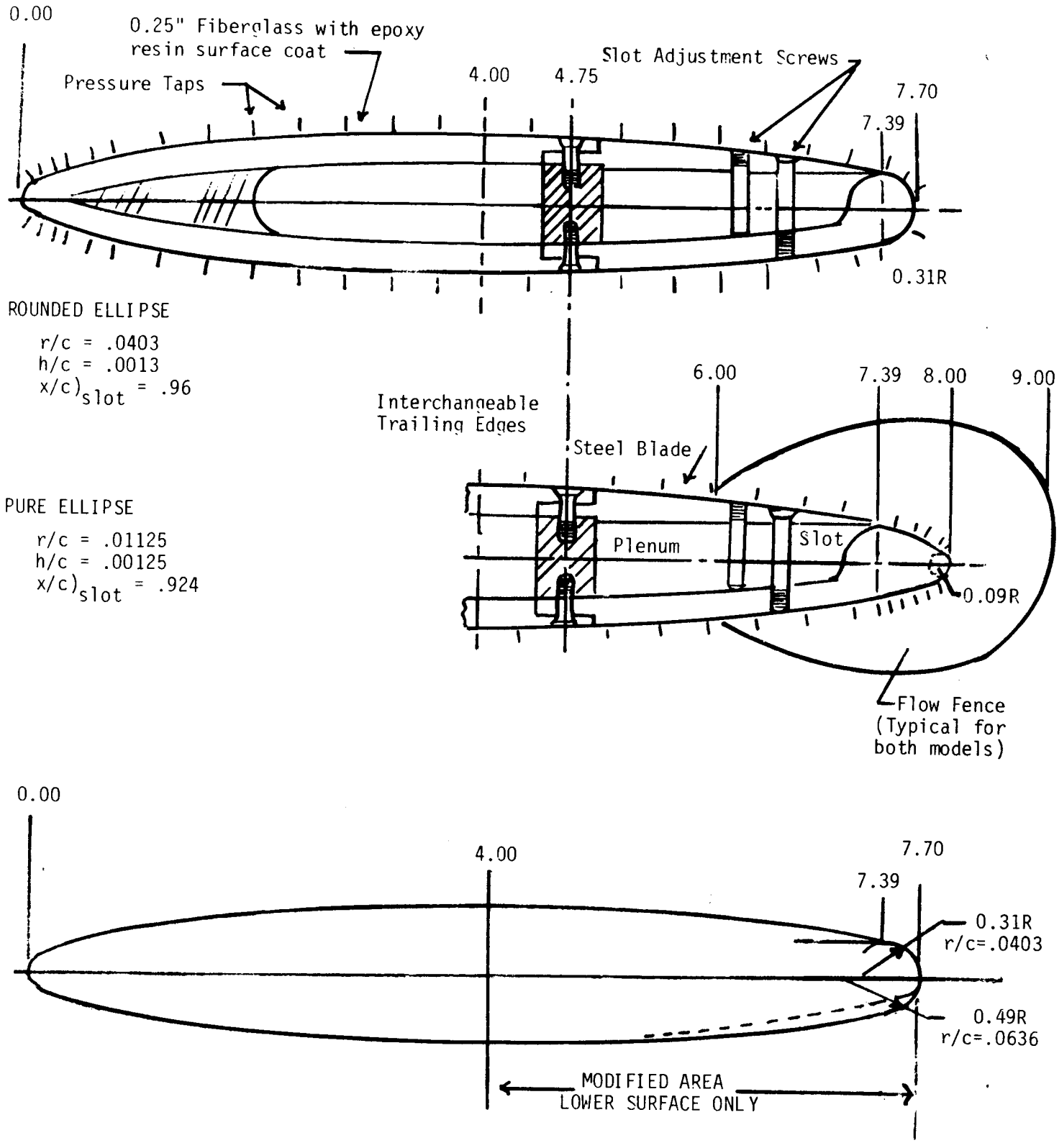

FIGURE 1. - AIRFOIL GEOMETRIES

All Dimensions in Inches (1 inch = 2.54 cm)

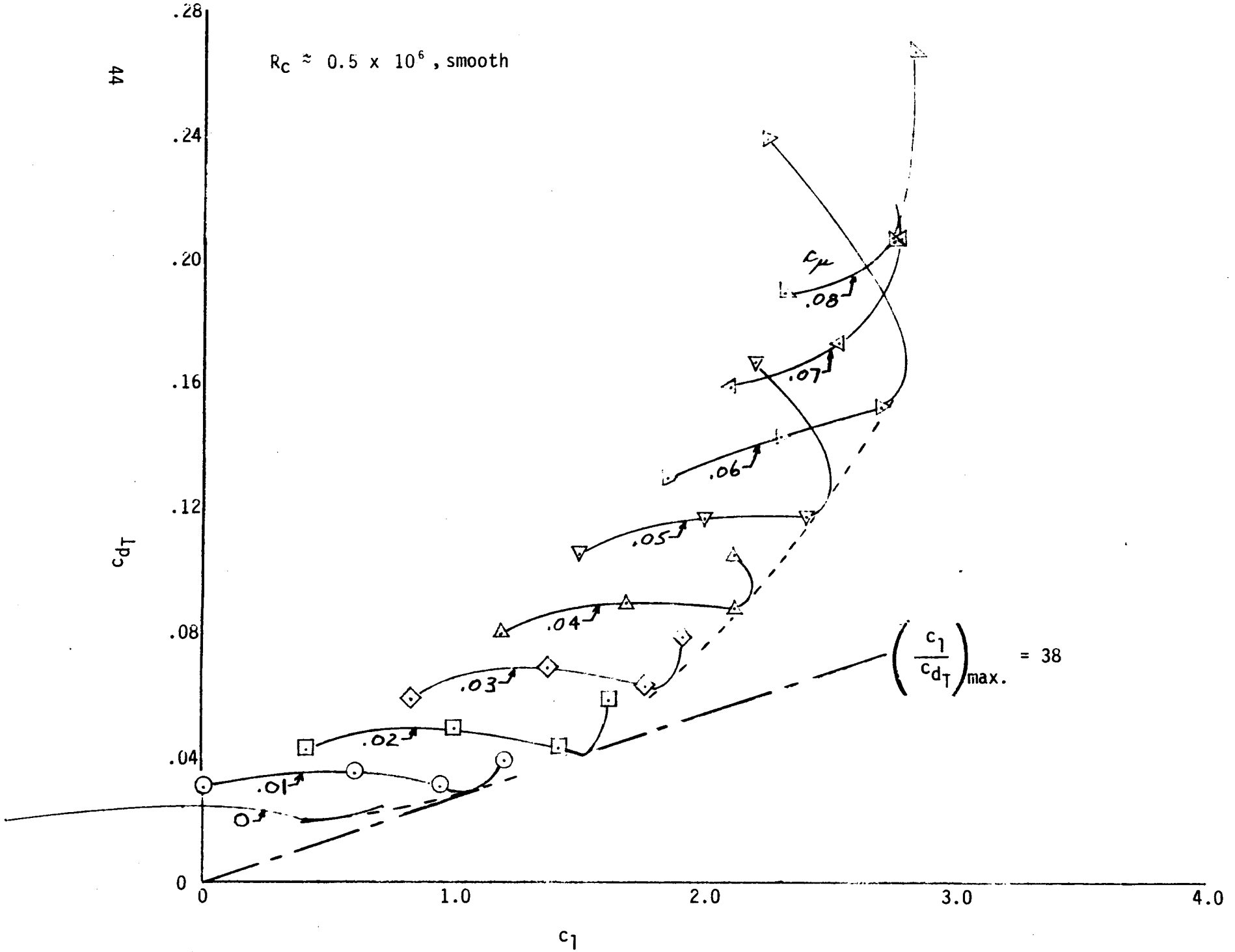

FIGURE 2. - VARIATION OF AIRFOIL TOTAL DRAG COEFFICIENT WITH AIRFOIL LIFT COEFFICIENT FOR ROUNDED 15-PERCENT CHORD THICK ELLIPSE

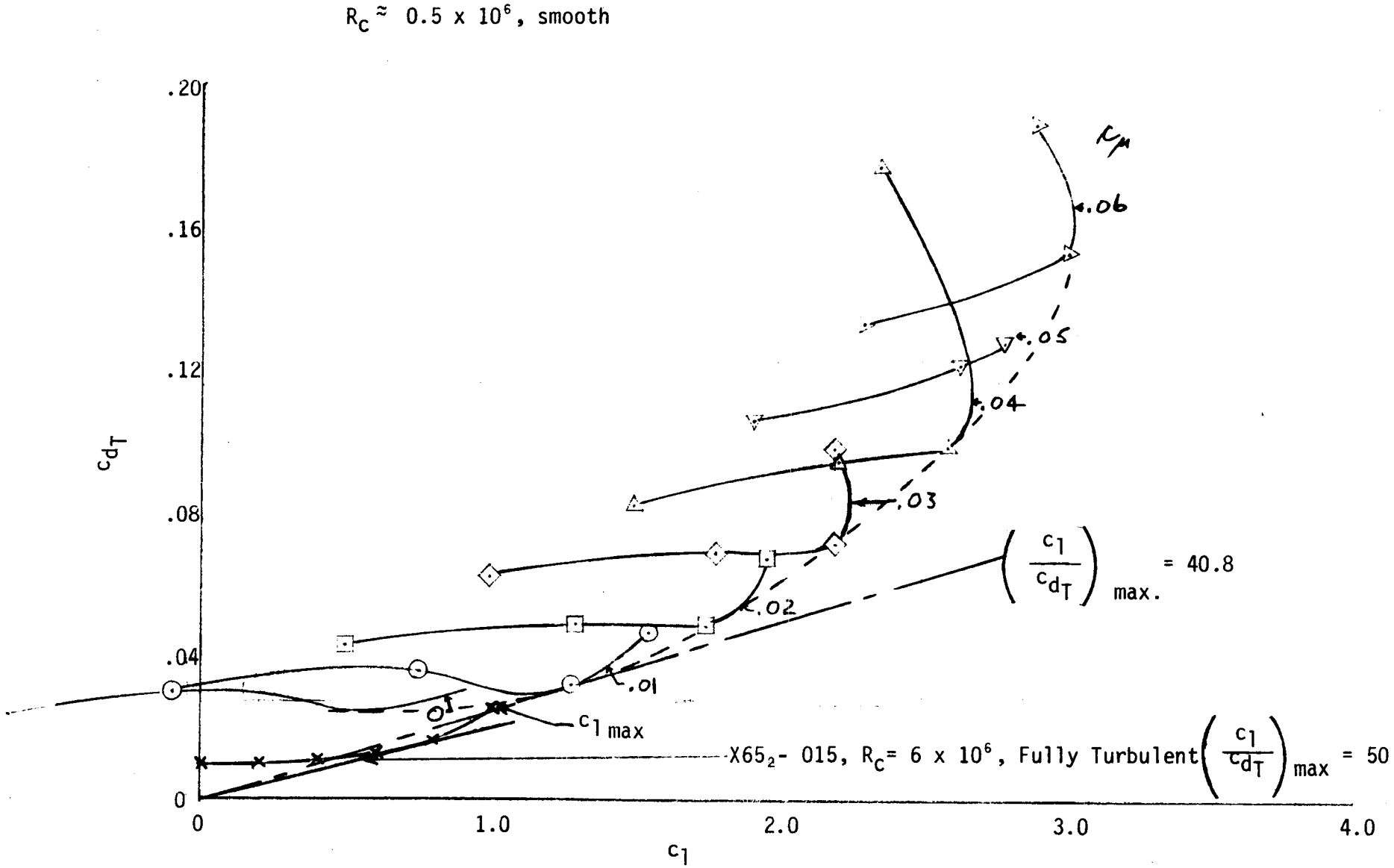

FIGURE 3. - VARIATION OF AIRFOIL TOTAL DRAG COEFFICIENT WITH AIRFOIL LIFT COEFFICIENT FOR MODIFIED 15-PERCENT CHORD THICK ELLIPSE

FIGURE 4. - VARIATION OF AIRFOIL LIFT COEFFICIENT WITH ANGLE OF ATTACK FOR ROUNDED 15-PERCENT CHORD THICK ELLIPSE

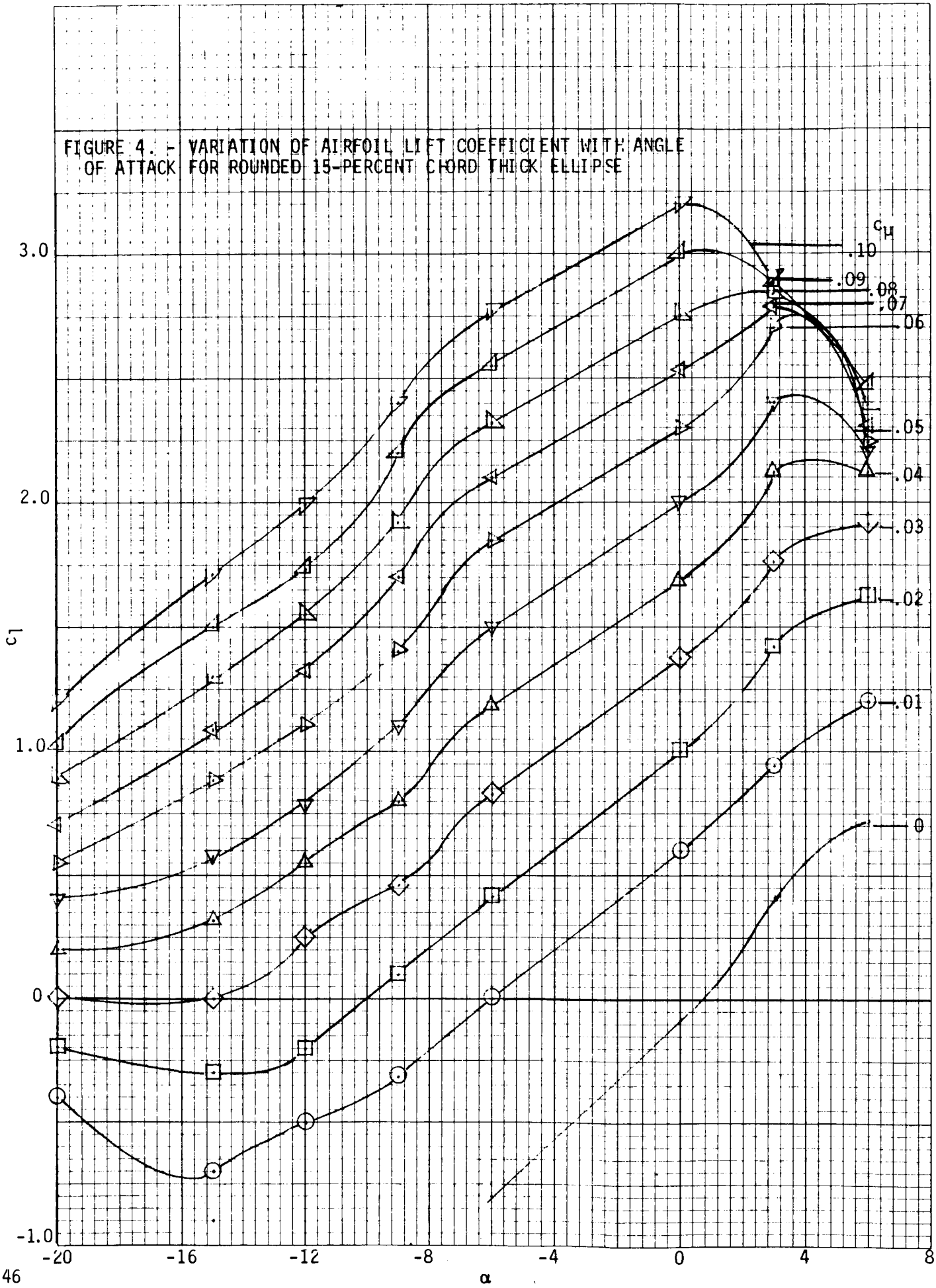

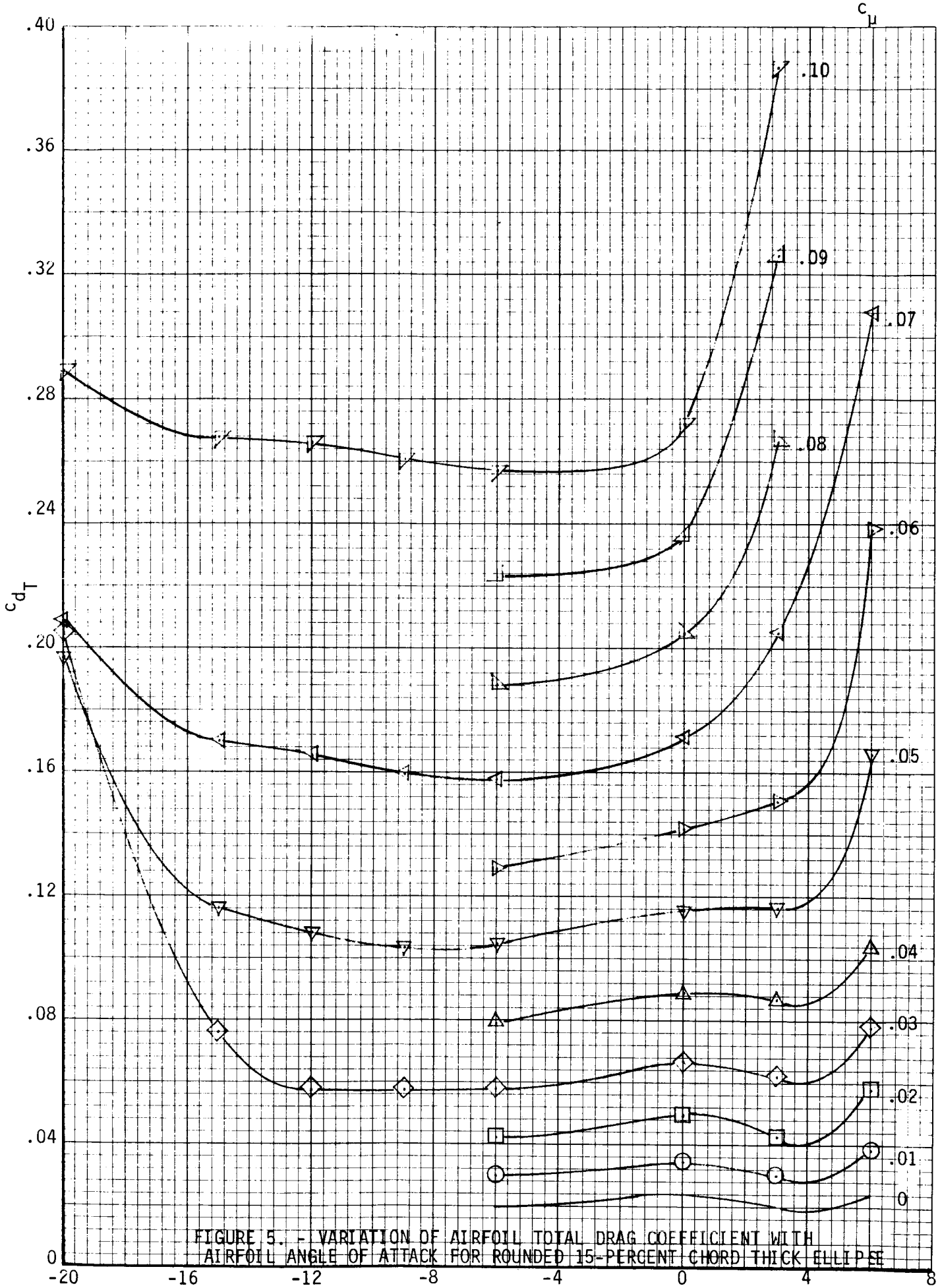

FIGURE 5. - VARIATION OF AIRFOIL TOTAL DRAG COEFFICIENT WITH AIRFOIL ANGLE OF ATTACK FOR ROUNDED 15-PERCENT CHORD THICK ELLIPSE

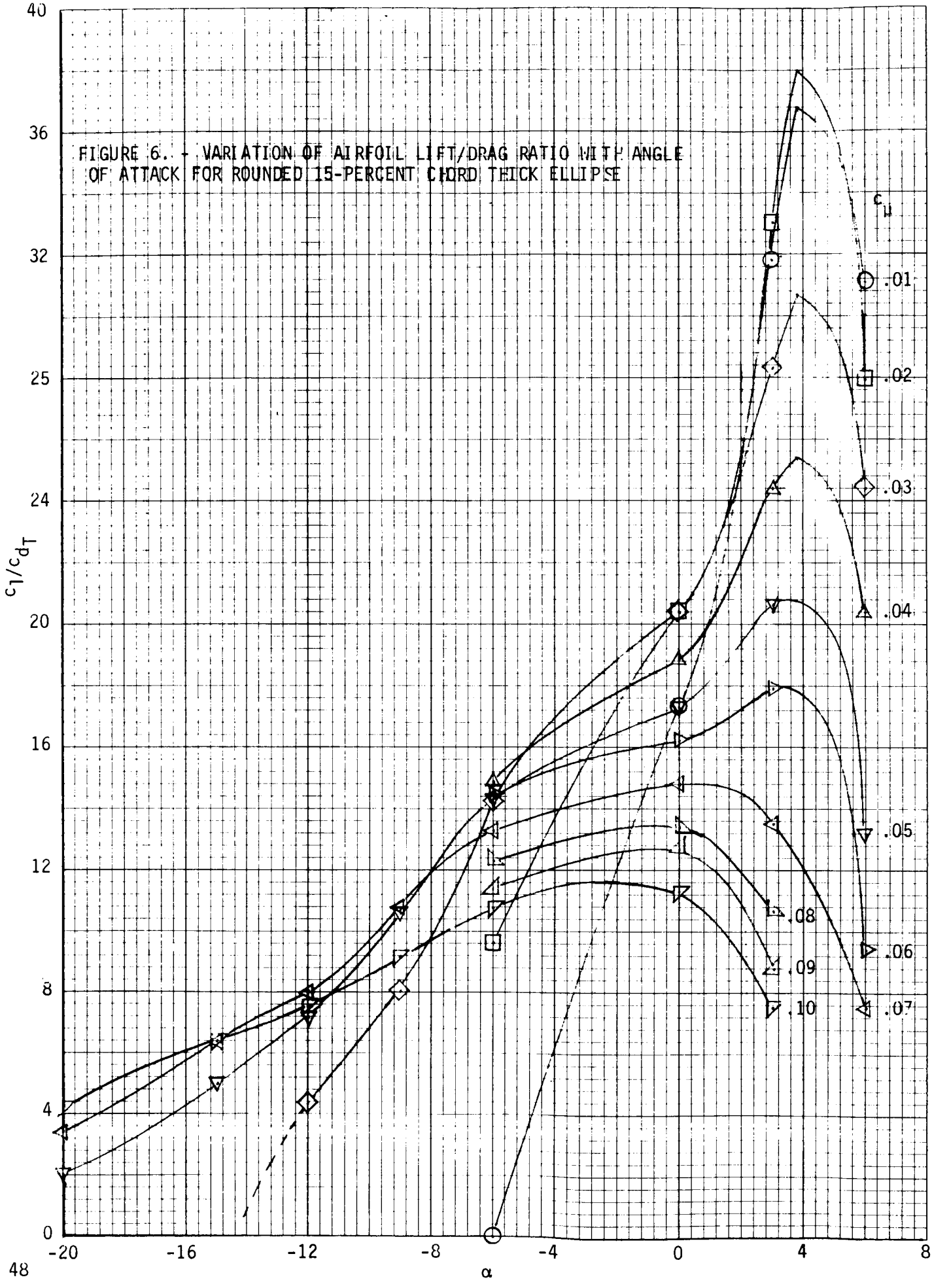

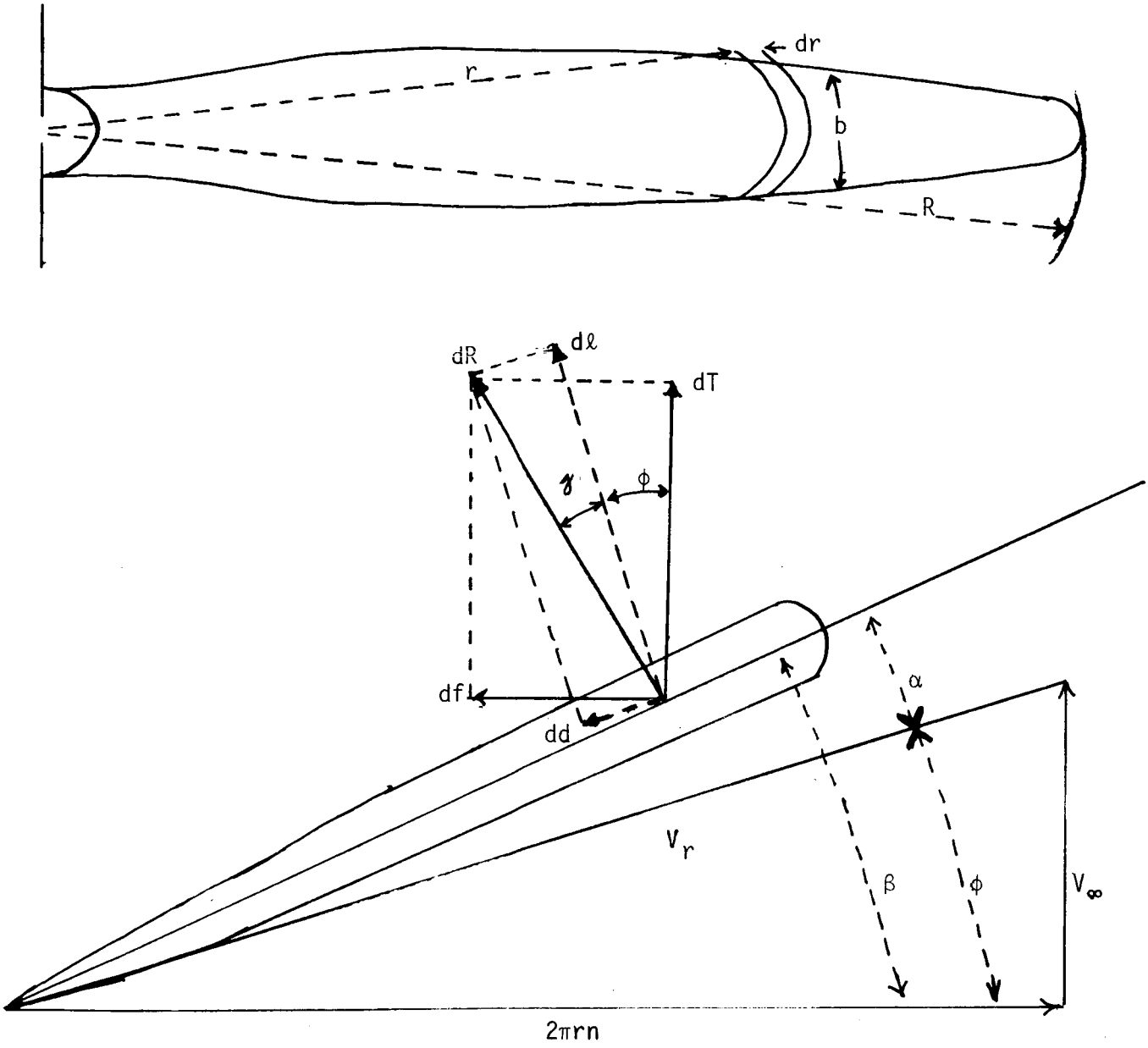

FIGURE 7. - PROPELLER BLADE ELEMENT DEFINITIONS

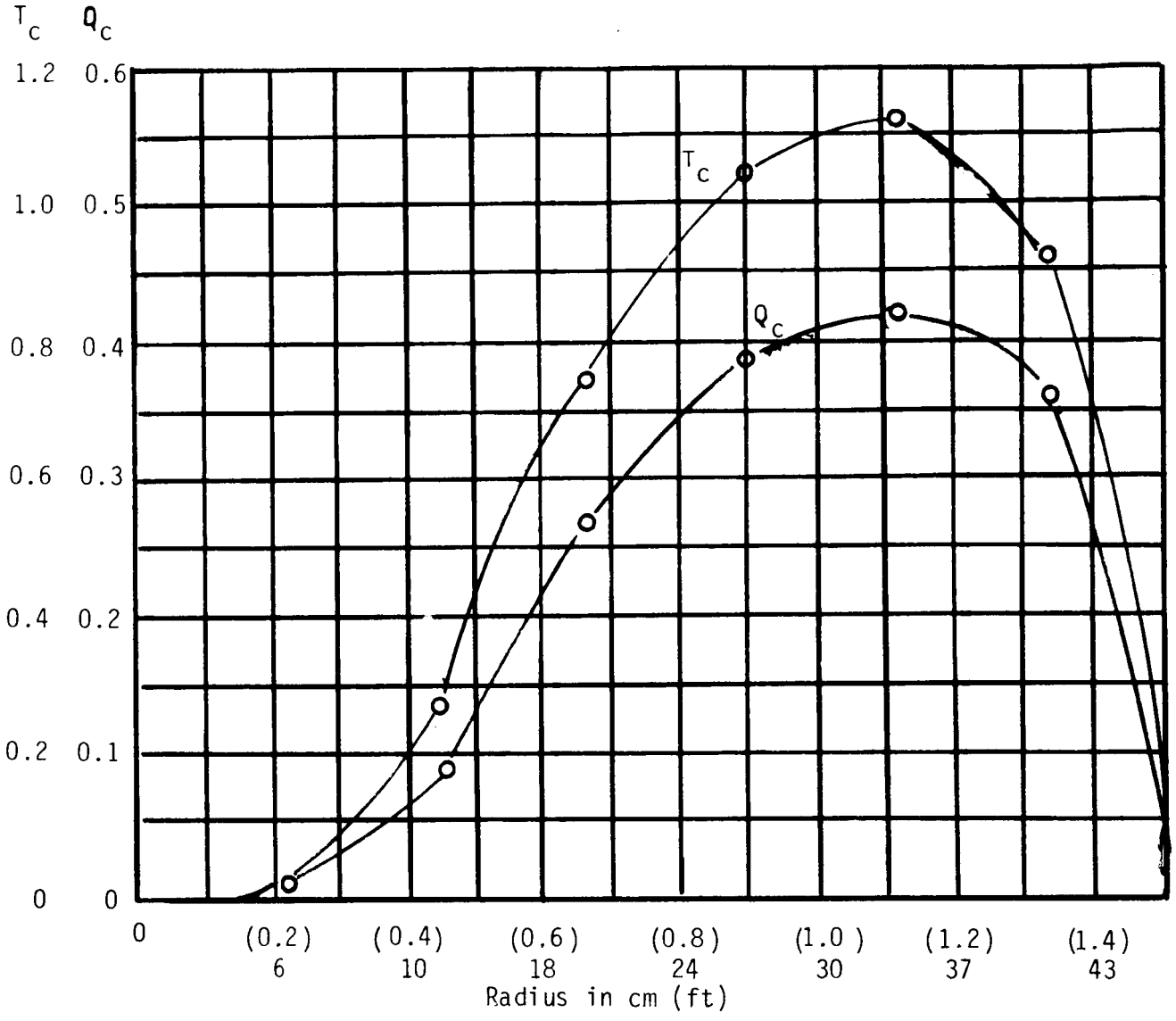

FIGURE 8. - THRUST AND TORQUE GRADING CURVES

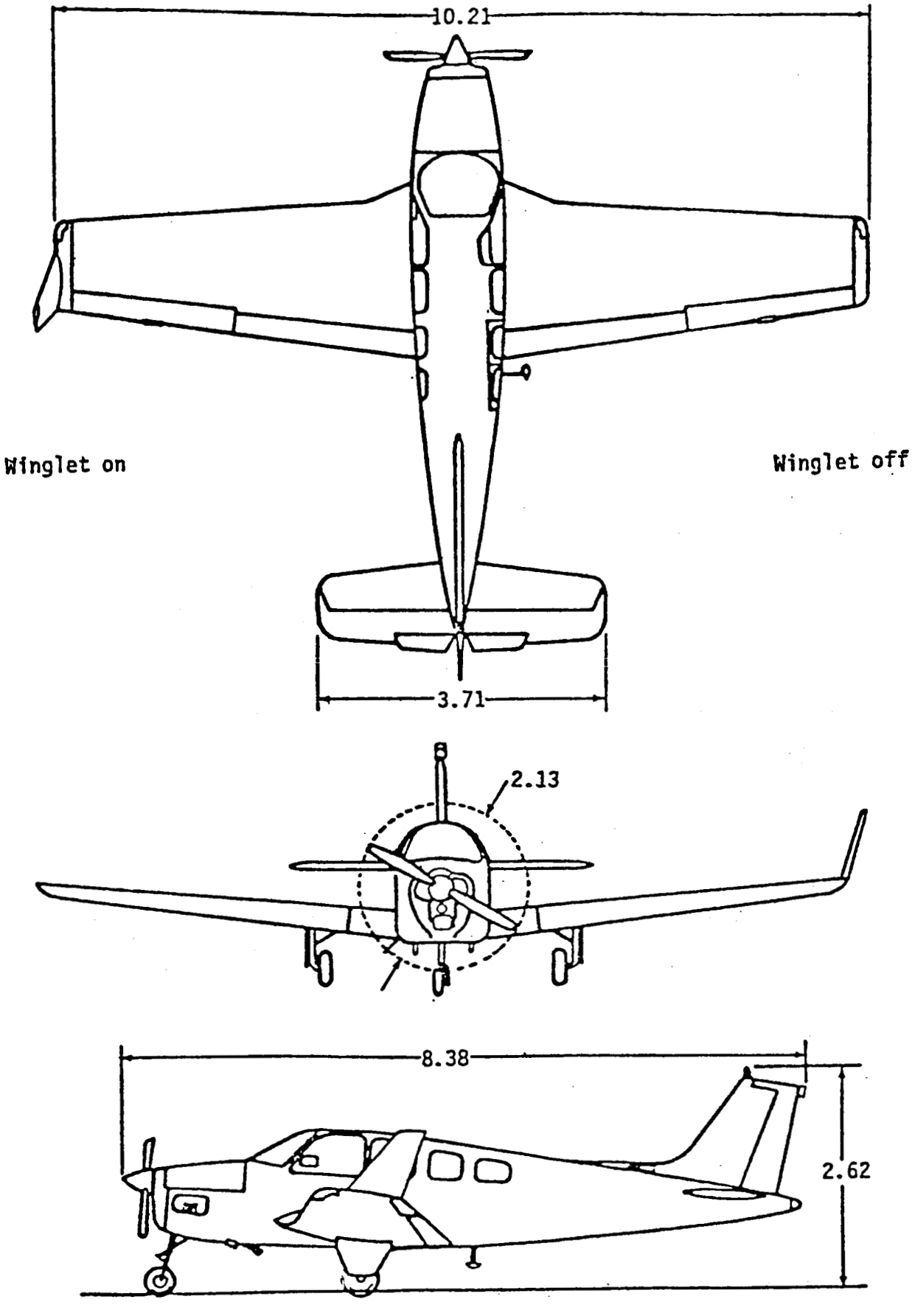

Dimensions In Meters

FIGURE 9. THREE VIEW OF SELECTED AIRPLANE

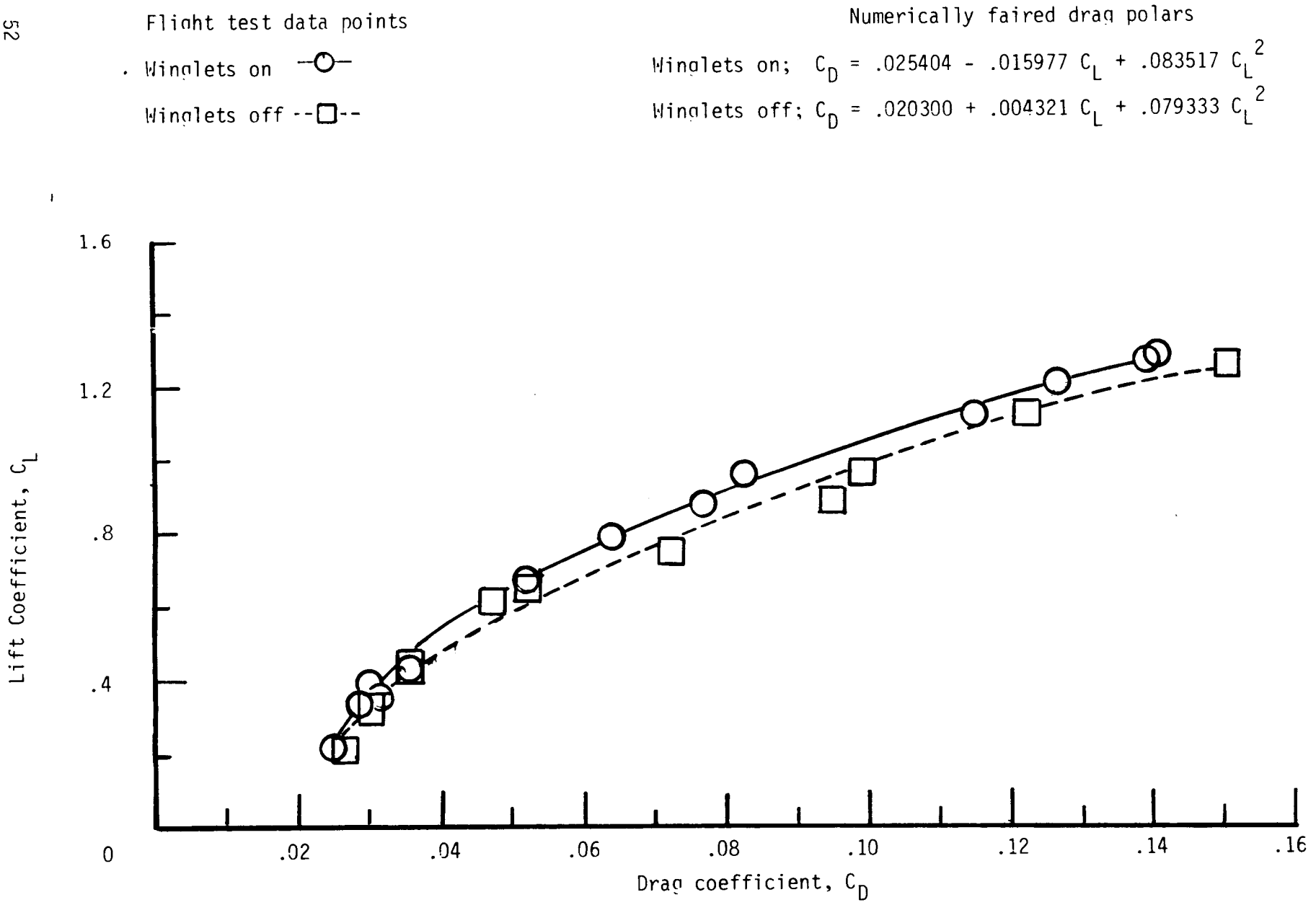

FIGURE 10. - VARIATION OF SELECTED AIRPLANE LIFT COEFFICIENT WITH AIRPLANE DRAG COEFFICIENT

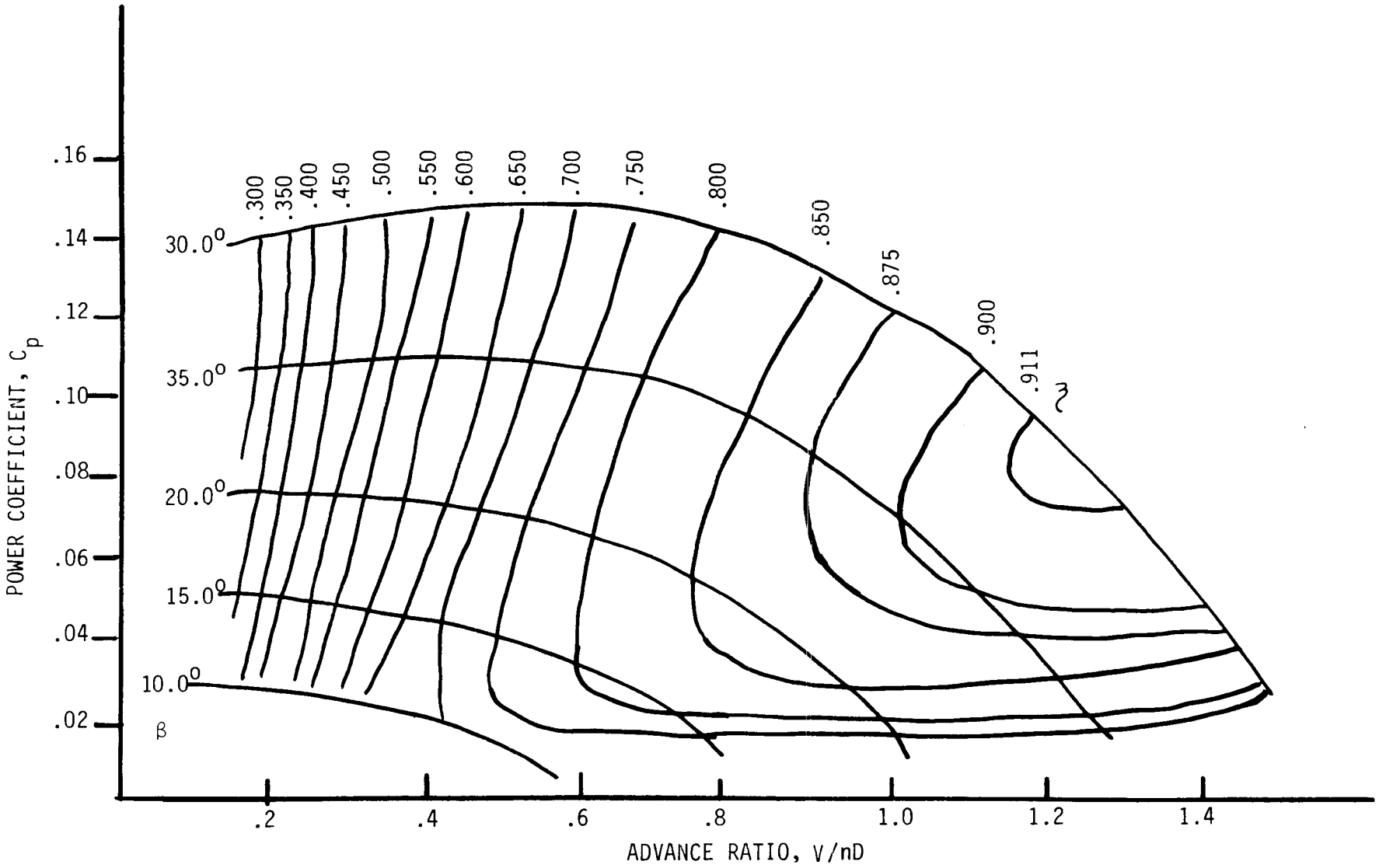

FIGURE 11. - VARIATION OF BASIC PROPELLER POWER COEFFICIENT WITH ADVANCE RATIO FOR SELECTED AIRPLANE

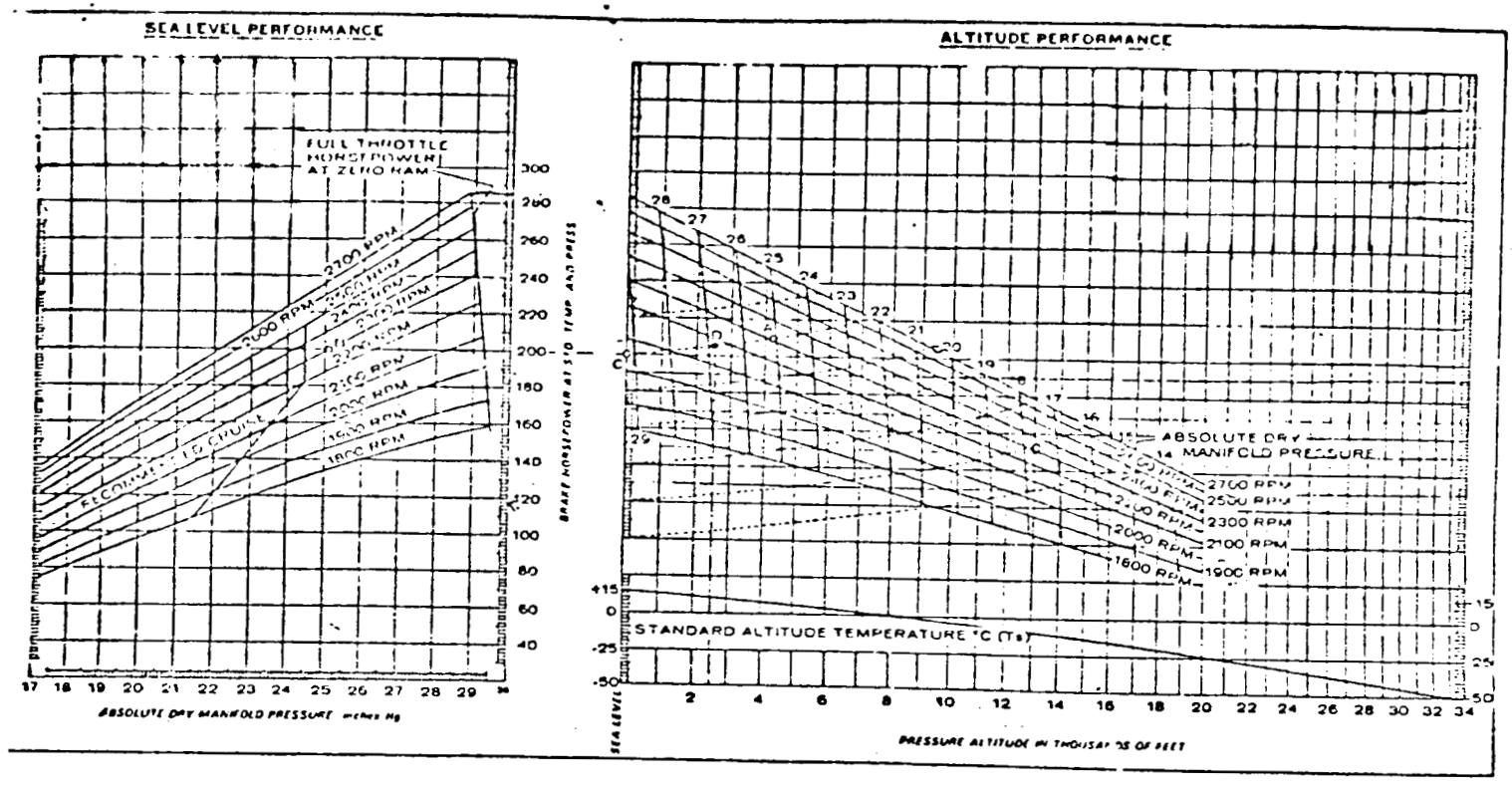

FIGURE 12. - ALTITUDE PERFORMANCE CURVES FOR SELECTED AIRPLANE ENGINE

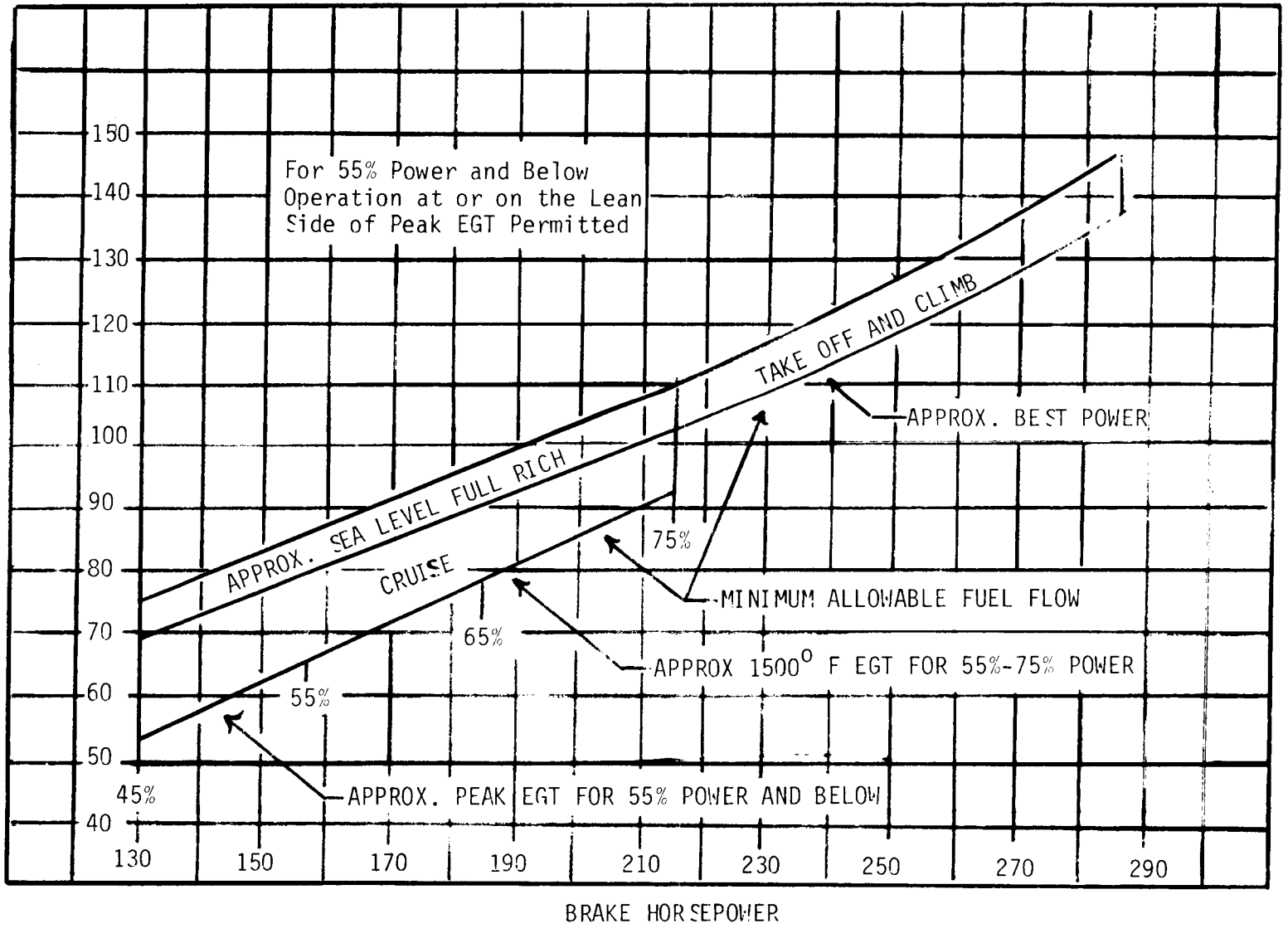

FIGURE 13. - FUEL FLOW CHARACTERISTICS FOR SELECTED AIRPLANE ENGINE

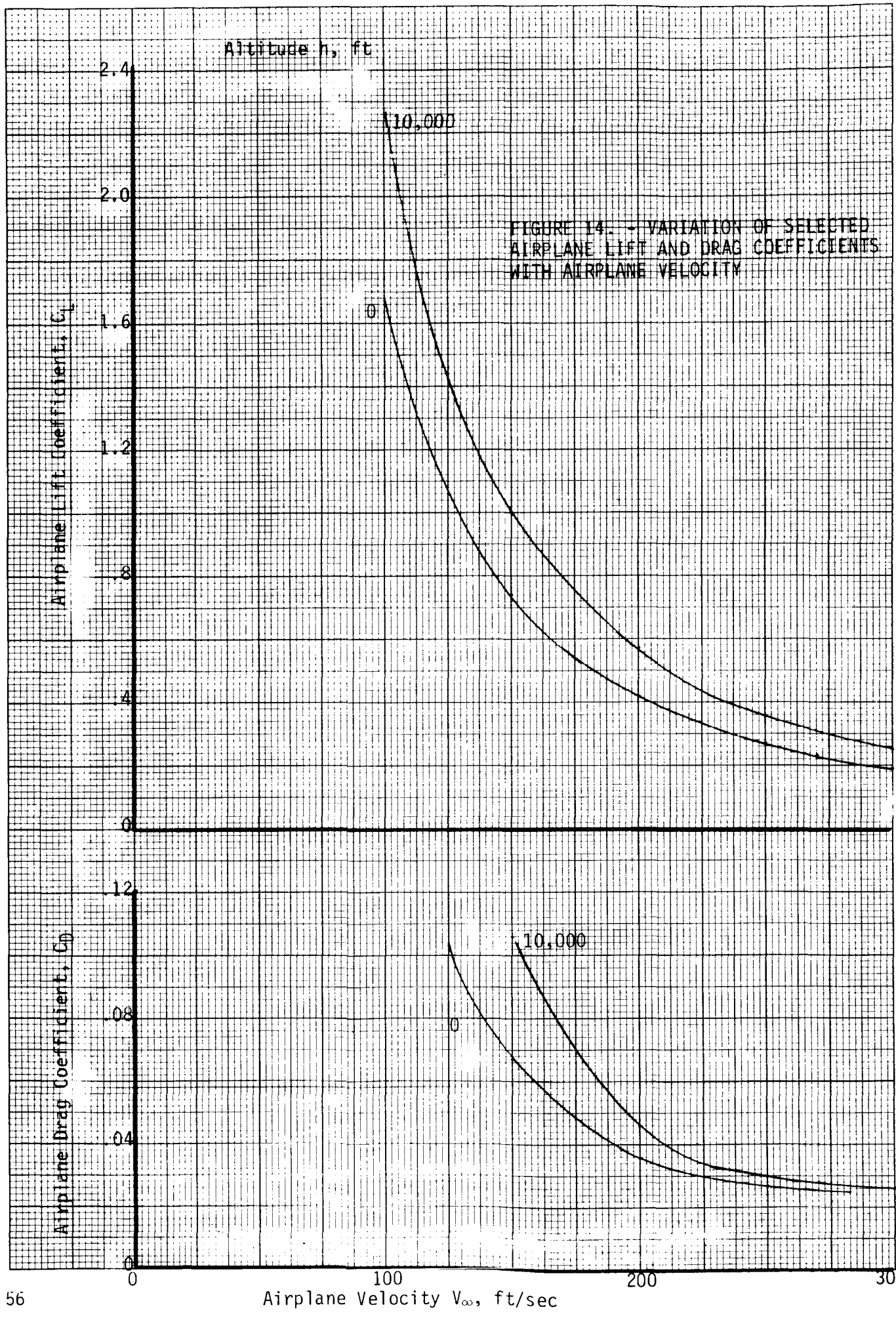

FIGURE 14. - VARIATION OF SELECTED AIRPLANE LIFT AND DRAG COEFFICIENTS WITH AIRPLANE VELOCITY

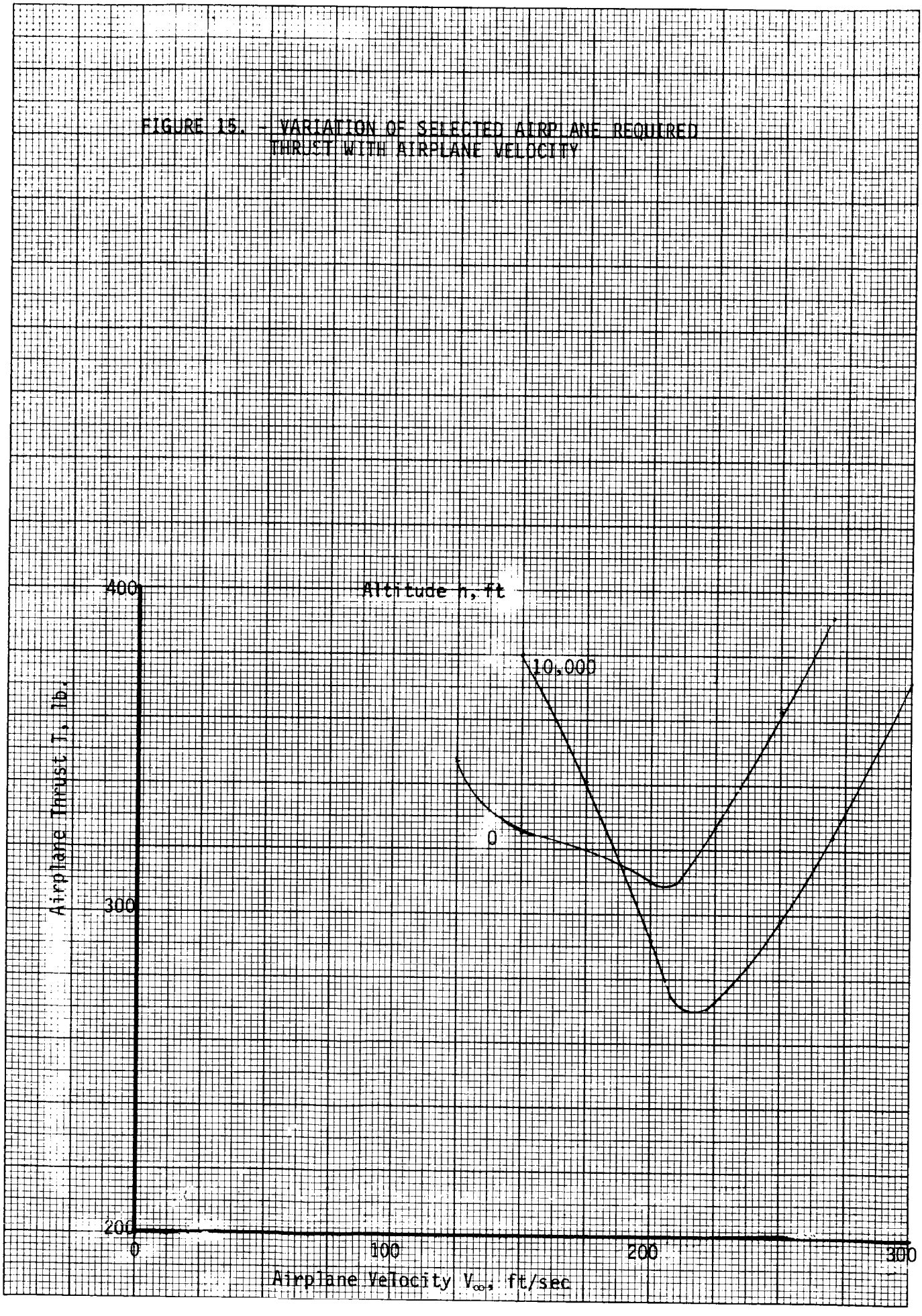

FIGURE 15. - VARIATION OF SELECTED AIRPLANE REQUIRED THRUST WITH AIRPLANE VELOCITY

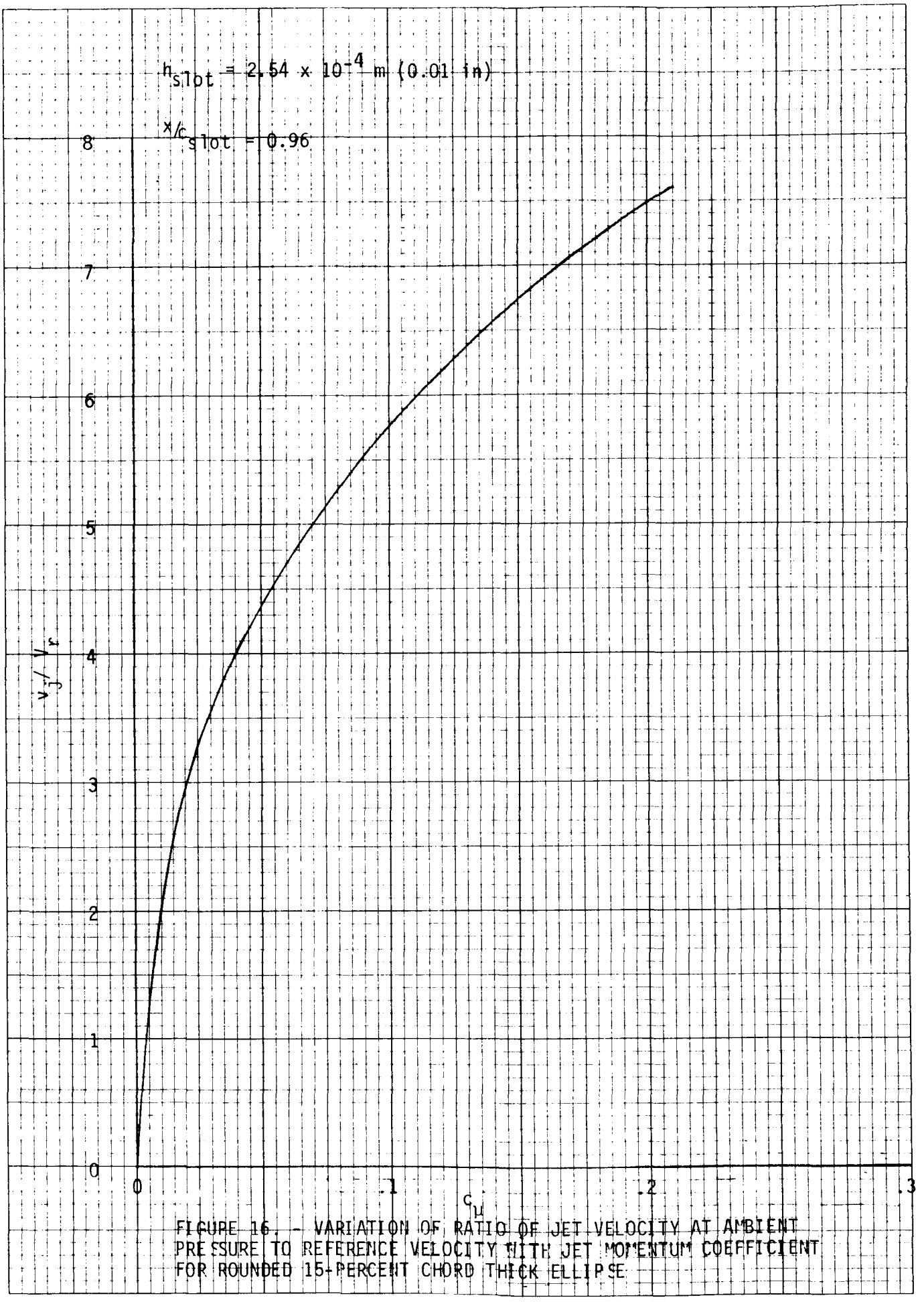

FIGURE 16. - VARIATION OF RATIO OF JET VELOCITY AT AMBIENT PRESSURE TO REFERENCE VELOCITY WITH JET MOMENTUM COEFFICIENT FOR ROUNDED 15-PERCENT CHORD THICK ELLIPSE

FIGURE 17. - VARIATION OF SELECTED AIRPLANE PROPELLER POWER COEFFICIENT AND THRUST COEFFICIENT WITH PROPELLER EFFICIENCY

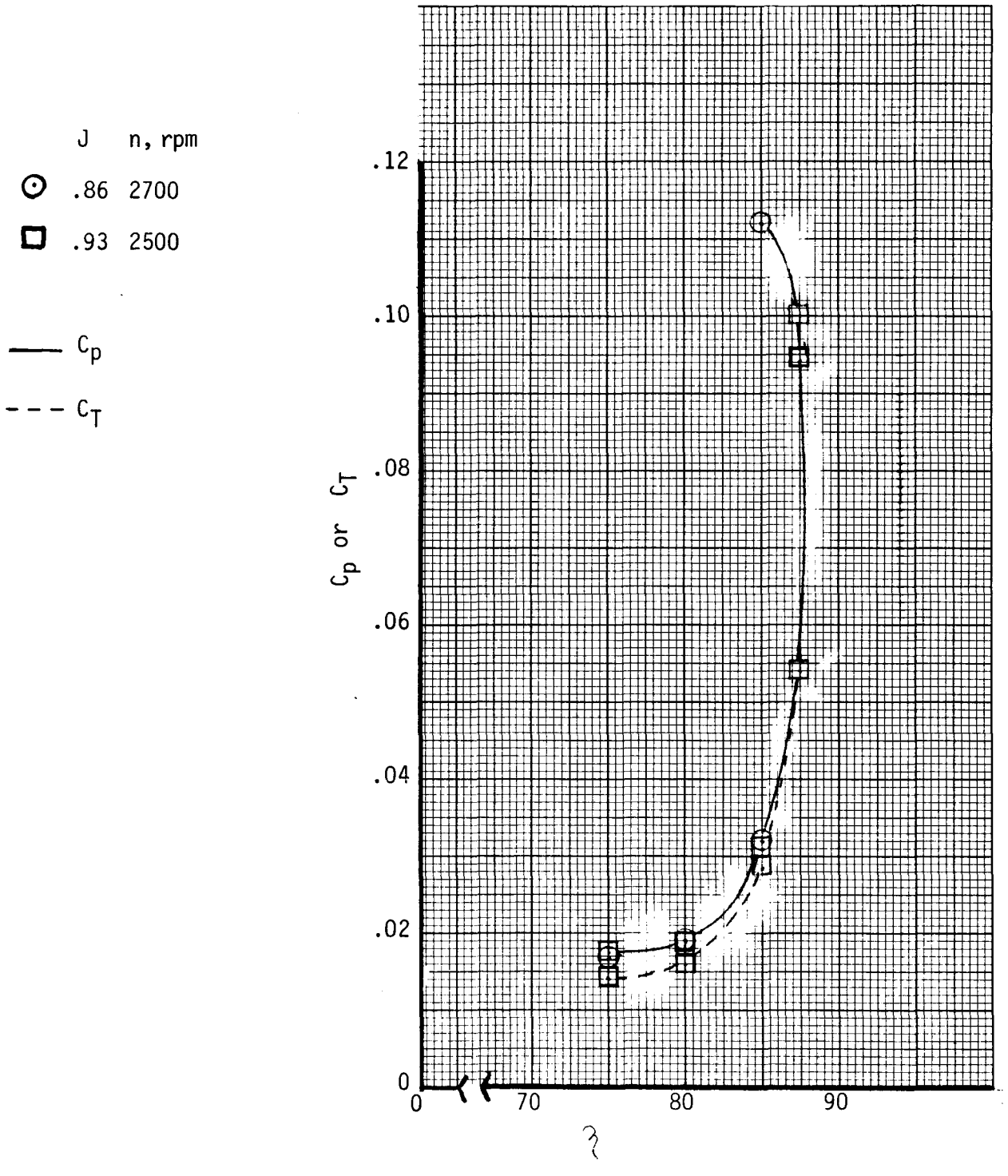

FIGURE 18. - 17-PERCENT CHORD THICK CIRCULATION-CONTROL SUPERCRITICAL AIRFOIL

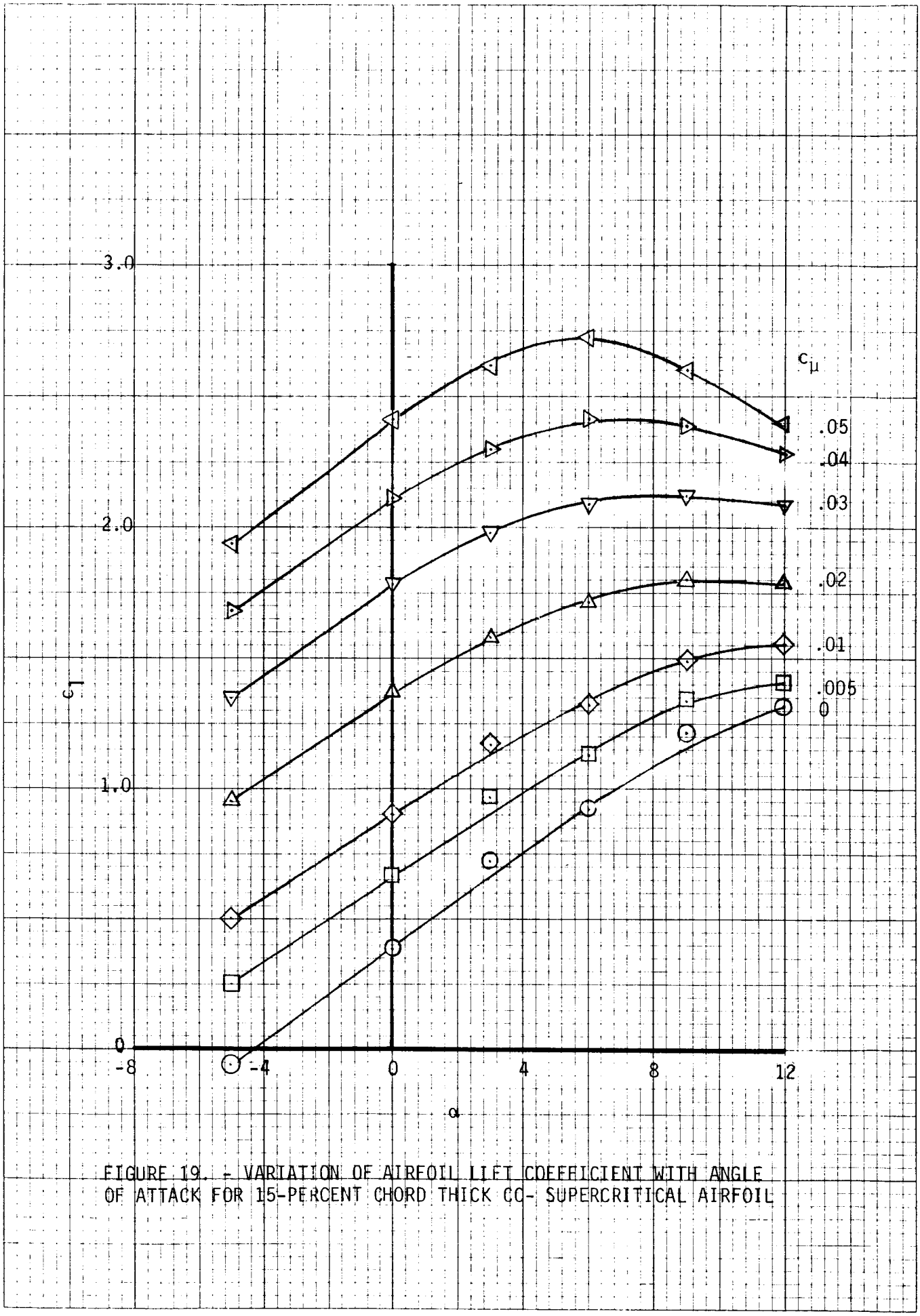

FIGURE 19. - VARIATION OF AIRFOIL LIFT COEFFICIENT WITH ANGLE OF ATTACK FOR 15-PERCENT CHORD THICK CO- SUPERCRITICAL AIRFOIL

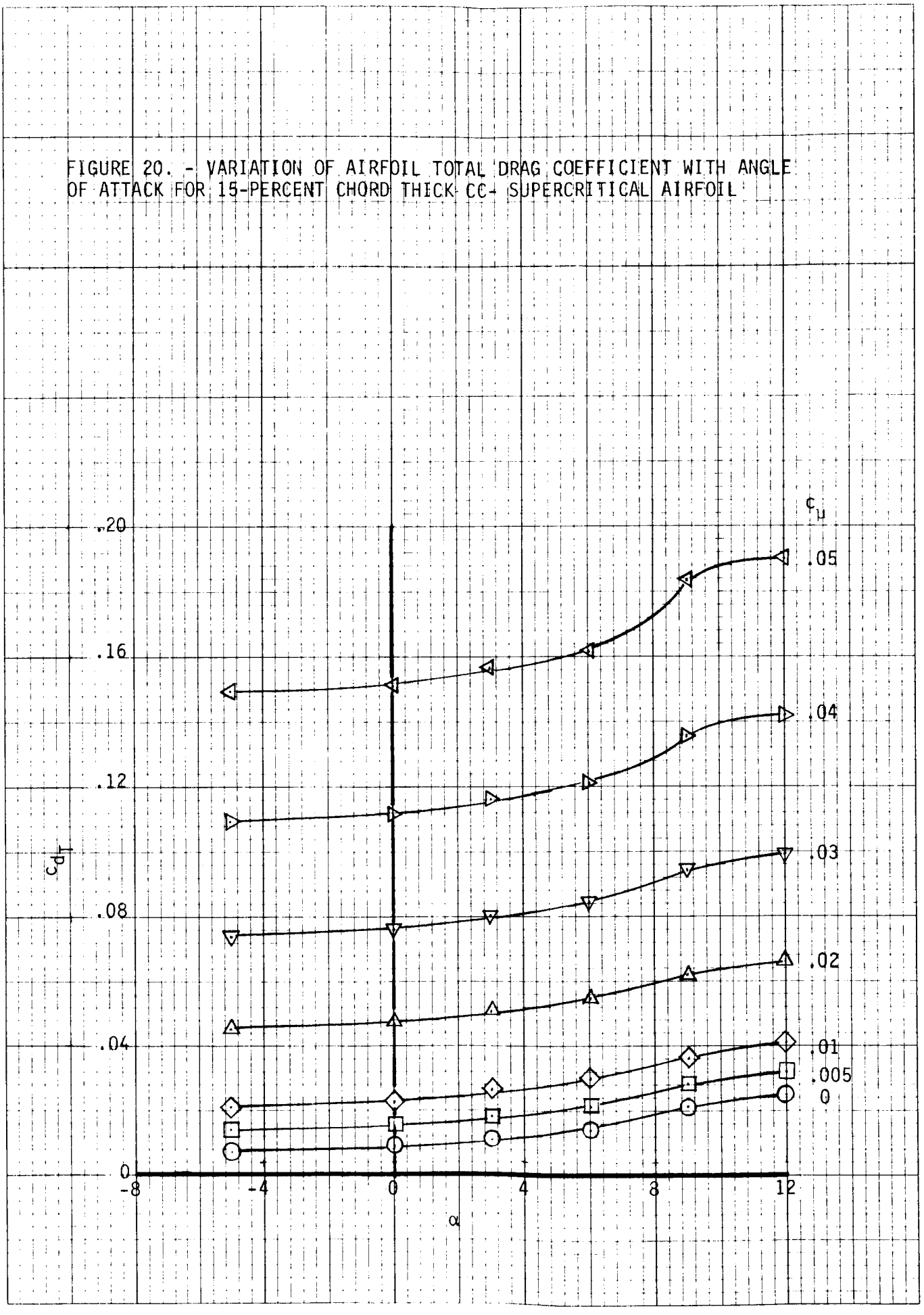

FIGURE 20. - VARIATION OF AIRFOIL TOTAL DRAG COEFFICIENT WITH ANGLE OF ATTACK FOR 15-PERCENT CHORD THICK CC- SUPERCRITICAL AIRFOIL

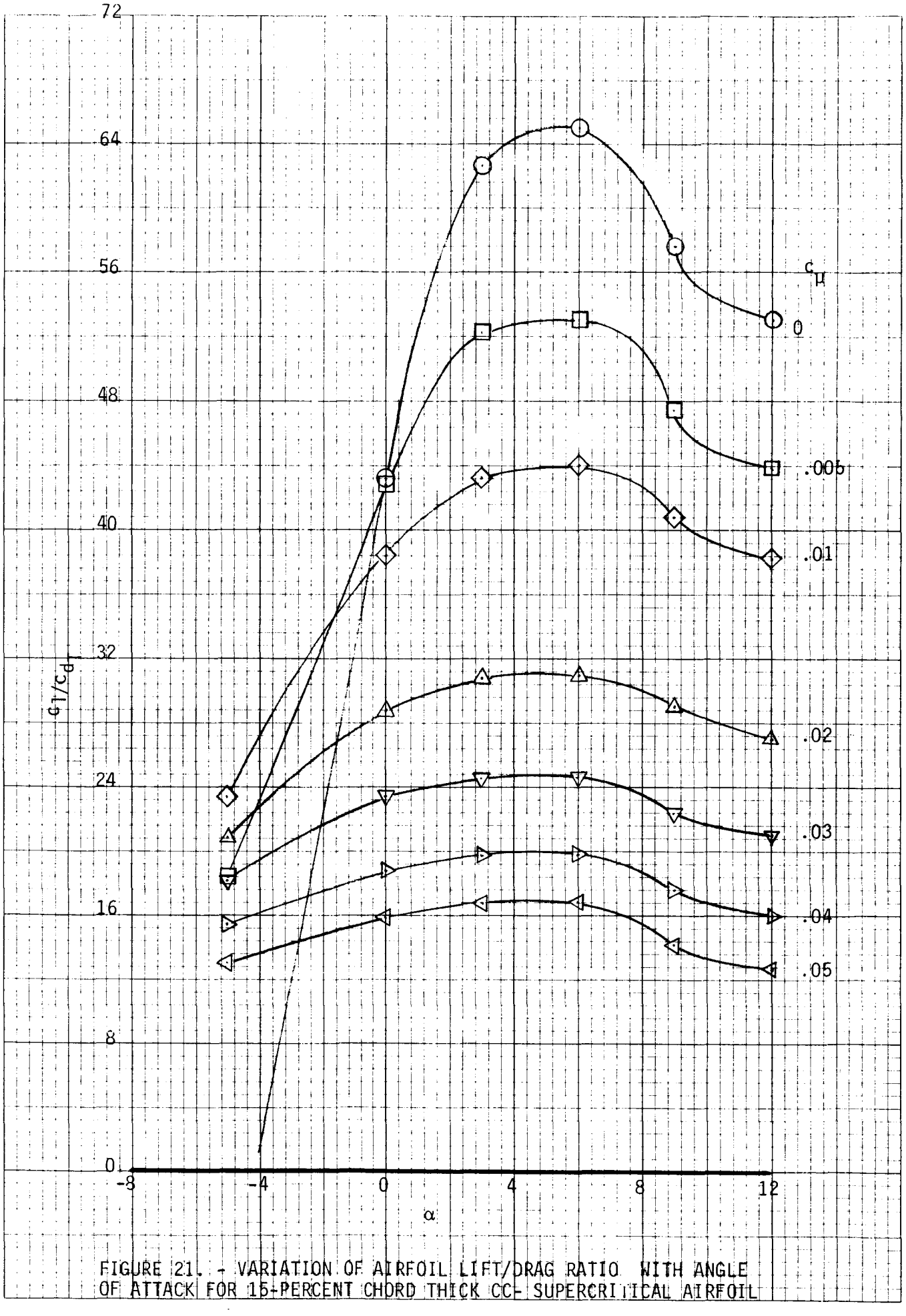

FIGURE 21. - VARIATION OF AIRFOIL LIFT/DRAG RATIO WITH ANGLE OF ATTACK FOR 15-PERCENT CHORD THICK CC- SUPERCRITICAL AIRFOIL

FIGURE 22. - VARIATION OF RATIO OF JET VELOCITY AT AMBIENT PRESSURE TO REFERENCE VELOCITY WITH JET MOMENTUM COEFFICIENT FOR 15-PERCENT CHORD THICK CC- SUPERCRITICAL AIRFOIL

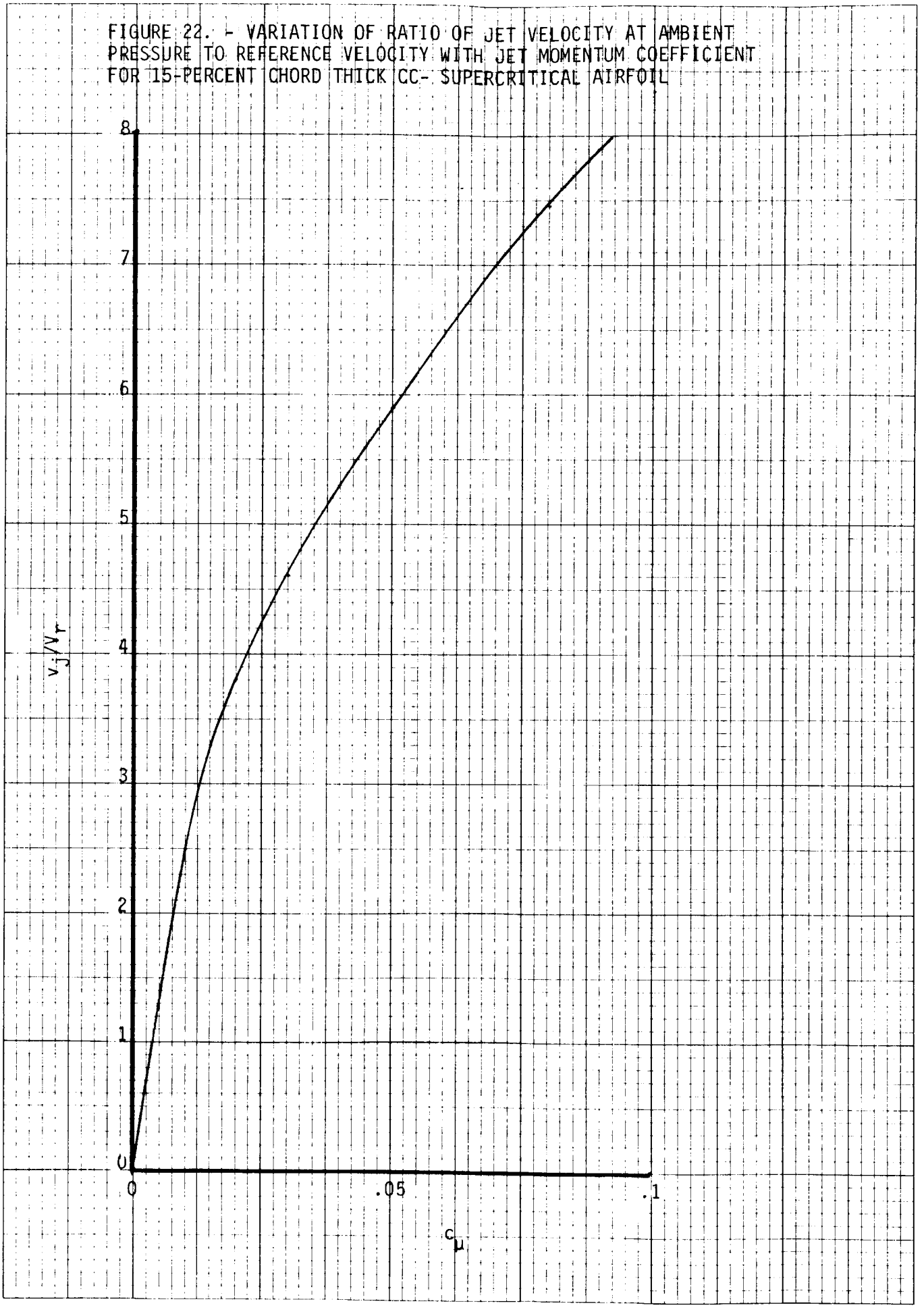

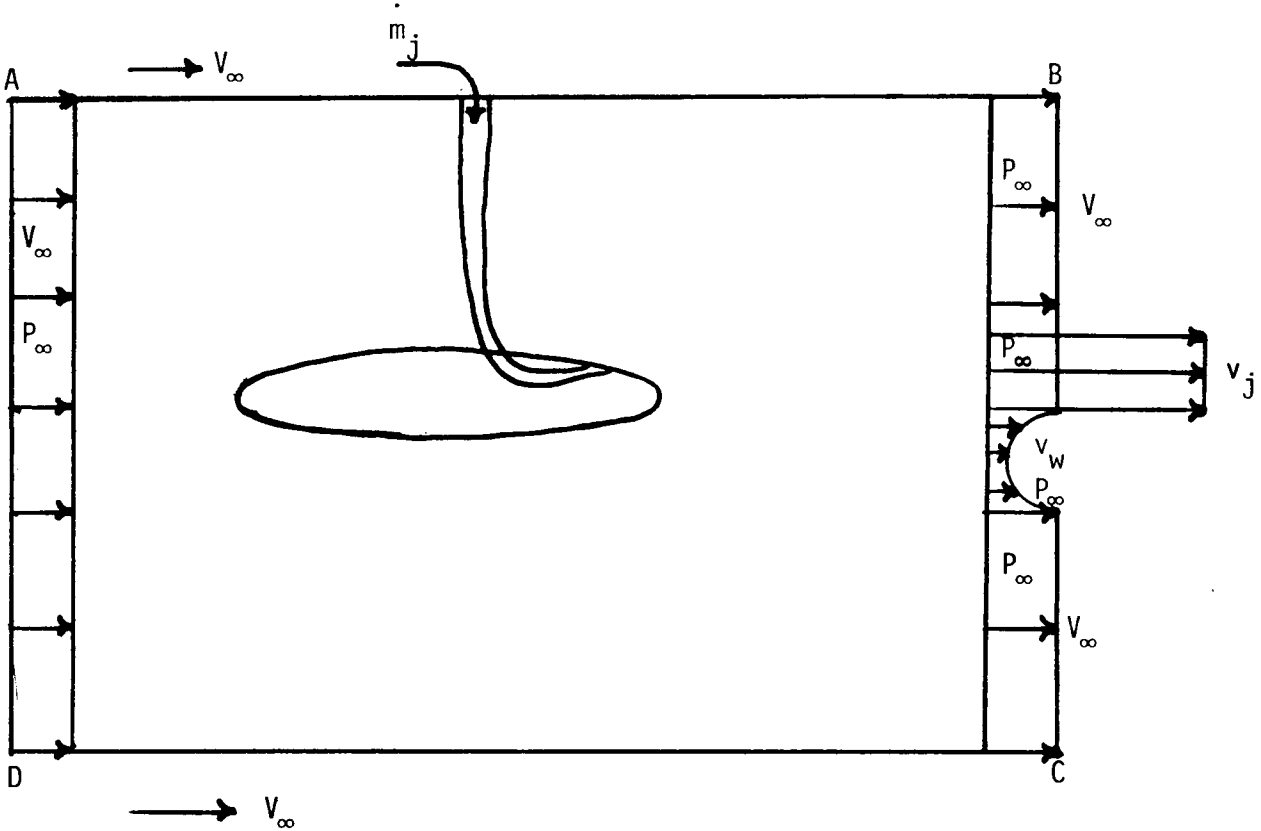

FIGURE A. 1. - REFERENCE PLANES FOR THE MOMENTUM EQUATION

$$c_{d_T} = \overbrace{c_{d_w} - \underbrace{\frac{\dot{m}_j\, v_j}{q_\infty\, S}}_{c_\mu}}^{c_{d_{rake}}} + \underbrace{\frac{\dot{m}_j\, V_\infty}{q_\infty\, S}}_{c_\mu \left(\frac{V_\infty}{v_j}\right)} + \overbrace{\underbrace{\frac{d_{pe}}{q_\infty\, S}}_{\frac{c_\mu}{2}\left(\frac{v_j}{V_\infty} - \frac{V_\infty}{v_j}\right)}}^{c_\mu \left(\frac{v_j}{V_\infty} + \frac{V_\infty}{v_j}\right)}$$

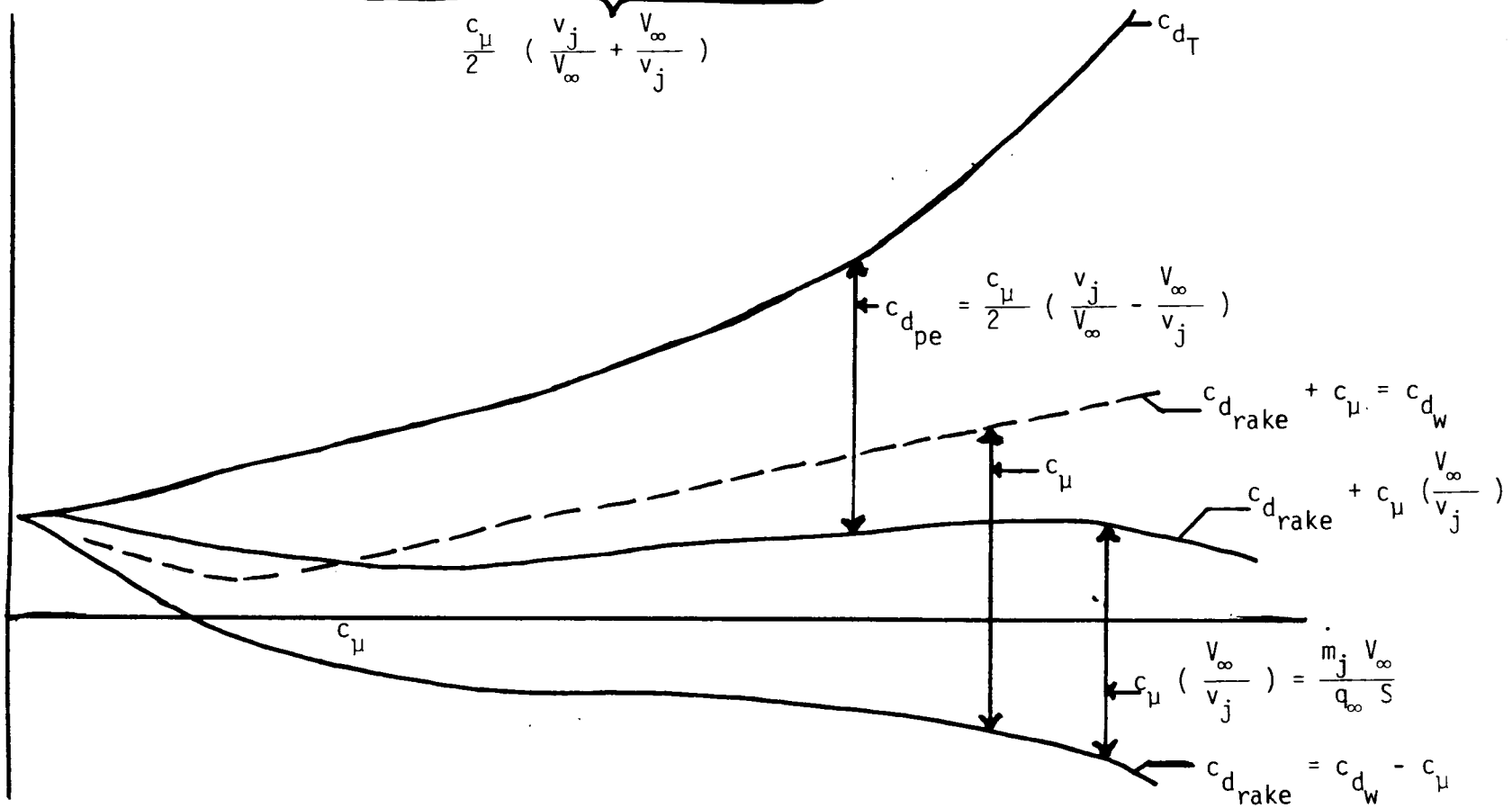

FIGURE A. 2. - SCHEMATIC OF CC AIRFOIL DRAG COEFFICIENT BREAKDOWN

1. Report No.	2. Government Accession No.	3. Recipient's Catalog No.
NASA CR-165748		

4. Title and Subtitle	5. Report Date
AERODYNAMIC EVALUATION OF CIRCULATION CONTROL PROPELLERS	June 1981
	6. Performing Organization Code

7. Author(s)	8. Performing Organization Report No.
Albert L. Braslow	
	10. Work Unit No.

9. Performing Organization Name and Address	11. Contract or Grant No.
The Bionetics Corporation 18 Research Drive Hampton, Virginia 23666	NAS1-14970
	13. Type of Report and Period Covered

12. Sponsoring Agency Name and Address	13. Type of Report and Period Covered
National Aeronautics and Space Administration Washington, D.C. 20546	Contractor Report
	14. Sponsoring Agency Code

15. Supplementary Notes

Langley Technical Monitor: David C. Grana

16. Abstract

The aerodynamic compatibility of fixed-pitch circulation-control (CC) propellers with the performance characteristics and requirements of a 1600 kg (3600 lb) single-engine variable-pitch propeller general aviation airplane was evaluated. The initial results with elliptical-shaped CC airfoils indicated that the feasibility of application to fixed-pitch propellers was doubtful for the class of airplane investigated (cruise speed of about 300 km/hr) and improbable for higher-speed airplanes. Supplemental data for a cambered circulation-control supercritical airfoil, which became available after completion of the initial evaluation, were subsequently analyzed and are included in the Addendum to this report. With the much superior aerodynamic characteristics of the CC-supercritical airfoil, elimination of variable pitch appears aerodynamically feasible for low-speed airplanes through the use of a moderate amount of upper-surface blowing near the trailing edge during cruise. Overall feasibility depends upon results of structural and systems-type analyses.

17. Key Words (Suggested by Author(s))	18. Distribution Statement
General Aviation Circulation-Control Propeller Coanda Effect Propellers	FEDD DISTRIBUTION Subject Category 07

19. Security Classif. (of this report)	20. Security Classif. (of this page)	21. No. of Pages	22. Price*
Unclassified	Unclassified	73	

*Available: NASA Industrial Applications Centers